CHAPTER 2:
CONCRETE MATERIAL MODEL

2.1 Introduction

The response of a reinforced concrete structure is determined in part by the material response of the plain concrete of which it is composed. Thus, analysis and prediction of structural response to static or dynamic loading requires prediction of concrete response to variable load histories. The fundamental characteristics of concrete behavior are established through experimental testing of plain concrete specimens subjected to specific, relatively simple load histories. Continuum mechanics provides a framework for developing an analytical model that describe these fundamental characteristics. Experimental data provide additional information for refinement and calibration of the analytical model.

The following sections present the concrete material model used in this investigation for finite element analysis of reinforced concrete beam-column connections. Section 2.2 presents the experimental data considered in model development and calibration. Section 2.3 presents several concrete material models that are typical of those proposed in previous investigations. Section 2.4 discusses the material model implemented in this study. Section 2.5 presents a comparison of observed and predicted concrete behavior for plain concrete laboratory specimens subjected to several different load histories.

2.2 Concrete Material Properties Defined by Experimental Investigation

In developing an analytical model to predict material response, consideration of the physical mechanism of behavior may facilitate the development process and simplify the model formulation. The physical mechanisms of response are most evident in the qualitative and quantitative data collected during material testing with simple load histories. However, given the concrete composition and mechanisms of response, there are particular issues that must be considered in assessing the results of an experimental investigation.

Standardized tests may be used to define material parameters such as compressive strength, elastic modulus, tensile strength, and fracture energy. Available experimental data describe the response of concrete subjected uniaxial cyclic compression and tensile loading as well as uniaxial reversed-cyclic loading. Experimental testing of plain and reinforced concrete elements may be used to characterize the response of plain concrete subjected to loading in shear. Additionally, data define the stiffness and strength of concrete subjected to multi-dimensional loading. The results of these experimental investigations define a data set that may be used in model development and calibration.

2.2.1 The Composition and Behavior of Plain Concrete

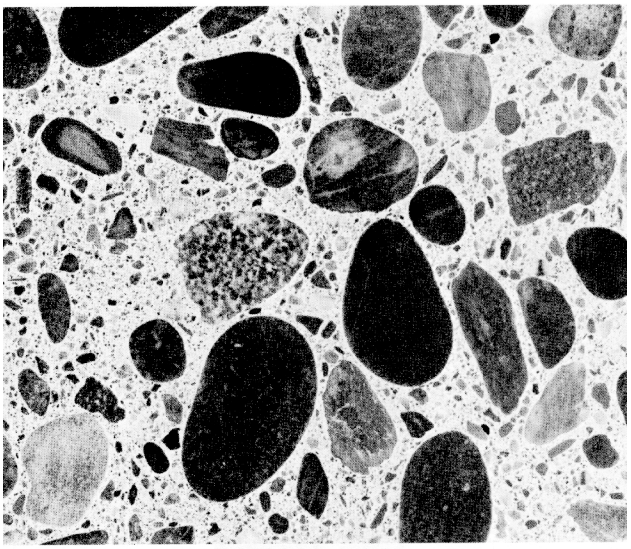

Figure 2.1: The Concrete Composite (from Mehta and Monteiro, 1993)

Plain concrete is a non-homogeneous mixture of coarse aggregate, sand and hydrated cement paste (see Figure 2.1). For normal-weight, normal-scale concrete mixes, coarse aggregate is usually gravel or crushed rock that is larger than 4.75 mm (0.187 in.) in diameter while sand is aggregate particles with diameters between 4.75 mm and 0.75 mm (0.187 in. and 0.029 in). Hydrated cement paste (*hcp*) refers to the hydration product of portland cement and water. The transition zone refers to the *hcp* located in the immediate vicinity of the coarse aggregate particles. Because the transition zone typically has a slightly higher water to cement ratio than is observed in the entire *hcp* and because of the physical boundary between the different materials, the transition zone is weaker than the remainder of the *hcp*.

The initiation and propagation of cracks is the dominant mechanism of concrete material response. Under moderate general loading, the response of the concrete mixture is controlled by microcracking in the transition zone between the aggregate and the *hcp.* Under increased loading, microcracks in the transition zone grow and merge and microcracks initiate in the *hcp*. Eventually, a continuous crack system forms that traverses the transition zone and the *hcp,* resulting in the loss of load capacity. Under compression type loading, the continuous crack system may include cracks that transverse the coarse aggregate. Under tensile loading, increased load acts directly to increase the stress at the crack tip and drive crack propagation. As a result, for tensile loading, the sequence of cracking leading up to the development of a continuous crack system and loss of strength occurs very rapidly. Increased compressive loading indirectly increases stress at the crack tip, driving crack propagation at a much slower rate. For compressive loading, the stages of crack initiation and propagation are readily identified in the observed concrete response, and loss of load capacity occurs more slowly.

2.2.2 Criteria for Experimental Investigation of Concrete Behavior

The composition of concrete and the mechanisms of concrete response, require particular consideration in assessing the experimental investigation of plain concrete behavior.

2.2.2.1 Consideration of the Analytical Model

Given that concrete is a non-homogeneous composite and that the primary mechanism of response is the development and propogation of discrete cracks, it is necessary to consider the general framework of the model in establishing the experimental data set.

The response of plain concrete can be modeled at the scale of the coarse aggregate with the model explicitly accounting for the response of the aggregate, the *hcp* and the

transition zone material as independent elements or as components of a composite [see Ortiz and Popov, 1982]. However, while there may be available experimental data that defines the response of aggregate and *hcp* to general loading, characterization of the transition zone must be accomplished indirectly. Further, the random nature of the component material properties and distribution adds complexity to models that are developed at this scale. In modeling the response of a reinforced concrete structural element, it is reasonable to incorporate both the microscopic response as well as the random nature of the concrete into a macromodel. The macromodel describes the response of a body of concrete that is many times the size of individual pieces of aggregate or of continuous zones of *hcp*. It is assumed that initially the concrete within the body is homogenous and that the material response of the components is represented in the global response of the concrete composite. For this investigation, plain concrete is idealized as an initially homogenous material.

The idealization of concrete as a homogeneous body requires additional consideration for the case of concrete subjected to moderate through severe loading. At these load levels, the response of concrete is determined by the formation of continuous crack systems. Some researchers have proposed models in which the idealization of concrete as a continuum is abandoned in the vicinity of a the crack, and crack systems are modeled discretely [*e.g.*, Ayari and Saouma, 1990; Yao and Murray, 1993]. Development and calibration of such a model requires experimental data defining the rate of crack propagation under variable stress states and load histories. Currently, there are few data available characterizing the concrete fracture process under multi-dimensional stress states. Additionally, such a model requires special consideration within the framework of a finite element program. Other researchers have shown that it is possible to maintain the idealization of concrete as a continuum in the presence of discrete cracks. In these models, the material damage (evident in reduced material strength and stiffness) associated with discrete crack-

ing is distributed over a continuous volume of the material. Such models include the fictitious-crack model [Hillerborg *et al.*, 1976], smeared-crack models [de Borst and Nauta, 1984], and the crack-band model [Bazant and Oh, 1983]. Modeling of concrete as a continuum results in a model that is compatible with many existing computer codes as well as provides a basis for application of existing continuum constitutive theory in developing models. For these reasons, in this investigation concrete is considered to be a continuum.

Modeling concrete as an initially homogeneous material and assuming that the discrete cracking is incorporated into a continuum model of concrete, it is necessary that the experimental data set on which the analytical model will be developed and calibrated be compiled from investigations that meet several criteria. The concrete specimens must have critical zones that are sufficiently large that the concrete composite in the vicinity is approximately a homogenous mixture. For load cases in which the material response is determined by a global mechanism (*e.g.*, microcracking) experimental measurement must define the deformation of the entire concrete body to ensure that the deformation is representative of the composite. For load cases in which the material response is determined by a local mechanism (*e.g.,* formation of a continuous crack surface), it is necessary that experimental measurement define the global deformation of the concrete body as well as the deformation associated with the localized mechanism. This allows for appropriate calibration of the continuum model.

2.2.2.2 Consideration of Experimental Methods

Under severe loading, concrete exhibits a softening response. In order to characterize concrete response through experimental testing, it is necessary that the experimental equipment and procedure meet particular criteria. These criteria are more complete than those required for testing of hardening materials. Specifically, it is necessary that the following requirements by satisfied:

1. Loading must be conducted using displacement control with a closed-loop system in order to maintain a uniform rate of loading.
2. The applied rate of loading must be representative of that which the actual specimen will experience in the field, or results must be adjusted to account for the effects of load rate.
3. The reaction frame must be sufficiently stiff that the frame deformation does not contribute to the prescribed deformation path of the material specimen.
4. It is necessary that the testing apparatus not contribute to undesirable loading of the specimens. For the tests introduced here, it may be sufficient to increase specimen size so that boundary conditions do not contribute to the stress state at the critical section. However, for some tests, it may be necessary to apply loads using brushes or to lubricate the contact surface of the specimens in order to reduce the undesirable stresses introduced at the specimen-load frame interface.

2.2.3 Concrete Material Parameters Defined through Standardized Testing

The prolific use of concrete in the construction industry has led to the development of a series of standardized testing procedures for determining concrete material properties. A concrete material model may be calibrated on the basis of material parameters determined using these standard procedures.

The response of a reinforced concrete structural element is determined in part by the response of plain concrete in compression. As a result, standard practice in the United States [ACI, 1992] recommends characterizing the response of concrete on the basis of the compressive strength of a 6 inch diameter by 12 inch long (150 mm by 310 mm) concrete cylinder. For typical concrete mixes, the standard cylinder is sufficiently large that the material is essentially homogeneous over the critical zone. Additionally, while the standard procedure (ASTM C39) does not require efforts to reduce frictional confinement induced during testing at the ends of the specimen, the specimen is considered to sufficiently long that approximately the middle third of the cylinder experiences pure compres-

sion. Thus, this method is appropriate for determining the uniaxial, compressive strength of concrete.

Following from the test for compressive strength, ASTM C469 establishes a procedure for determining concrete elastic modulus. This method requires loading of the standard cylinder in uniaxial, cyclic compression at relatively low load levels. Some researchers have suggested that the *elastic* modulus for concrete may be different under compression and tension type loading. While it is possible that differences in microcrack patterns and distribution may affect material stiffness under compression and tension loading, it is likely that some difference in concrete response under compression and tension loading is due to the difference in boundary conditions under variable loading. For this investigation, concrete elastic material response, in tension and compression, is defined by a single set of material parameters established by standard material testing. In the absence of experimental data, the concrete elastic modulus may be estimated on the basis of the compression strength:

$$E_c = 33 w_c^{1.5} f_c^{0.5} \tag{2-1}$$

where E_c is the elastic modulus (psi), w_c is the weight density of the concrete (lb/ft^3) and f_c is the compressive strength (psi) [ACI, 1992].

Poisson's ratio characterizes the elastic response of concrete. Poisson's ratio can be determined experimentally by measuring the radial or circumferential expansion of a standard concrete cylinder subjected to compression loading. ASTM C469 establishes a standardize procedure for determination of Poisson's ratio from compression testing of standard cylinders. Most research suggests that Poisson's ratio for concrete is between 0.15 and 0.20 [*e.g.*, Mehta and Monteiro, 1993] and that there is little correlation between Poisson's ratio and other material properties. Mehta and Monteiro [1993] suggest that Poisson's ratio is generally lower with high strength concrete and lower for saturated and

dynamically tested concrete. However, Klink [1985] proposes, on the basis of extensive experimental testing, that an average value of Poisson's ratio appropriately is estimated on the basis of concrete compressive strength:

$$\nu_c = 4.5\times10^{-7} w^{1.75} f_c^{0.5} \tag{2-2}$$

where ν_c is the elastic Poisson's ratio, w_c is the unit weight of the concrete (lb/ft^3) and f_c is the compressive strength (psi). The value of Poisson's ratio predicted by Equation (2-2) varies between 0.16 and 0.20 for normal-weight, average-strength concrete. Given the observed variation in concrete composition and in experimental data, in the absence of experimental data a value of Poisson's ratio between 0.15 and 0.20 is appropriate for characterizing elastic material response.

Direct tension testing of concrete requires specialized equipment, procedures and consideration of boundary conditions. As a result, it is rarely performed. Instead, either the third-point flexural test (ASTM C78) or the splitting tension test (ASTM C496) is used to estimate concrete tensile strength. The flexural test consists of loading a plain concrete beam (150 by 150 by 500 mm) at the third points in flexural. The concrete tensile strength determined from this test, f_{ctfl}, is known to overestimate the direct tensile strength, f_{ct}, and is not appropriate for model calibration. However, the CEB-FIP Model Code (1993) recommends the following relationship for use in estimating the direct tensile strength, f_{ct}, on the basis of the flexural tensile strength, f_{ctfl}:

$$f_{ct} = f_{ctfl} \frac{2.0(h/h_o)^{0.7}}{1 + 2.0(h/h_o)^{0.7}} \tag{2-3}$$

where h is the depth of the beam in mm and h_o is 100 mm. The splitting cylinder test consists of applying a distributed line load to opposite long sides of a standard cylinder. The result of this loading is the development of an approximately uniform tensile stress distribution along the diameter of the cylinder between the applied loads. The tensile strength

as computed from this test has been found to overestimate the results of direct tensile testing by about 10 to 15 percent [Mehta and Monteiro, 1993]. This discrepancy may be corrected by reducing the tensile strength as defined by the splitting tensile test for use in model calibration. In the absence of experimental data, concrete splitting tensile strength may be predicted from the concrete compressive strength using the following relationship:

$$f_{ctsp} = 1.38(f_c)^{0.69} \quad \text{[Oluokun, 1991]} \tag{2-4}$$

where f_{ctsp} is the concrete splitting tensile strength (psi) and f_c is the concrete compressive strength (psi). Also, direct concrete tensile strength may be estimated on the basis of the concrete compressive strength using the following relationship:

$$0.95\left(\frac{f_c}{f_{co}}\right)^{2/3} \le f_{ct} \le 1.85\left(\frac{f_c}{f_{co}}\right)^{2/3} \quad \text{[CEB-FIP Model Code, 1993]} \tag{2-5}$$

where f_{ct} is the concrete direct tensile strength in MPa, f_c is the concrete compressive strength in MPa and f_{co} is 10 MPa. Energy dissipated during the brittle failure of concrete may be considered a material property and used in the calibration of material models. This energy, referred to as the concrete fracture energy, defines the energy required generate a unit area of crack surface. A commonly accepted procedure for experimental determination of concrete fracture energy is that proposed by RILEM 50-FMC Committee [1985]. In this procedure a notched concrete beam is subjected to three-point bending to failure and the applied load is controlled to produce a constant rate of crack width opening. It is assumed that all deformation of the beam in excess of that at the maximum load results from crack opening. Thus, the concrete fracture energy is defined as the integral of the stress versus deformation history for deformation is excess of that corresponding to the strength. For normal-weight, normal-sized concrete mixes, fracture energy as determined in accordance with the standard procedures varies from 0.090 MPa-mm to 0.230 MPa-mm [Monteiro *et al.*, 1993; Kozul and Darwin, 1997]. There is no apparent correlation

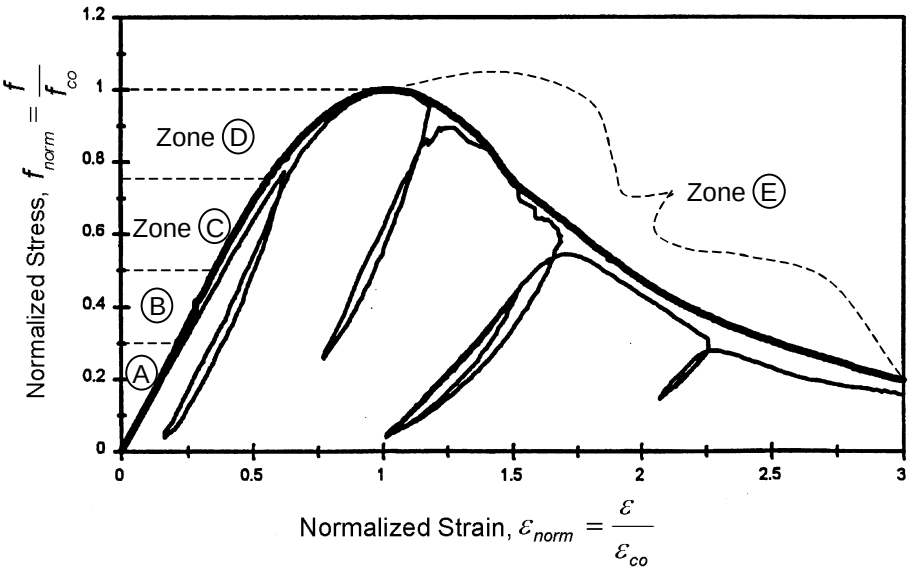

Figure 2.2: Concrete Response to Monotonic and Cyclic Compression Load (Data from Bahn and Hsu, 1998)

between fracture energy and compression or tension strength, although the data presented by Kozul and Darwin shows concrete mixtures with basalt coarse aggregate to have significantly higher fracture energy than those with limestone.

2.2.4 Concrete Subjected to Uniaxial Compression

The complete stress-strain history for concrete subjected to uniaxial compression provides data for use in characterizing the response of concrete to general loading. Figure 2.2 shows a plot of the stress-strain response of a typical concrete mix subjected to monotonically increasing compressive strain. Important characteristics of this response include the following outlined by Mehta and Monteiro [1993] (see Figure 2.2):

1. The response of the plain concrete under increasing strain is essentially linear-elastic until the load reaches approximately 30 percent of the peak compressive strength (Zone A). This linear-elastic response corresponds to minimal, stable crack growth within the transition zone. Note that a stable crack does not continue to grow under constant load.
2. Loading to compressive stress between 30 and 50 percent of peak compressive stress, results in some reduced material stiffness (Zone B). Reduction in the mate-

rial stiffness results from a significant increase in crack initiation and growth in the transition zone. Crack growth is stable.

3. Loading to compressive stress between 50 and 75 percent of peak compressive stress results in further reduction in material stiffness (Zone C). Here the reduced stiffness is partly a result of crack initiation and growth in the *hcp*. Additionally, reduced material stiffness results from the development of unstable cracks that continue to grow when subjected to a constant load.
4. Concrete loaded to more that 75 percent of the peak compressive load responds with increased compressive strain under constant loading (Zone D). This results from spontaneous crack growth in the transition zone and *hcp* and well as from the consolidation of microcracks into continuous crack systems.
5. Loading to compressive strains beyond that corresponding to the compressive strength results in reduced compressive strength (Zone E). This response is a result of the development of multiple continuous crack systems.

For model development, this behavior may be simplified into three levels of response. Concrete initially responds as an elastic material. Under increased loading, global microcracking results in reduced material stiffness. Eventually, further increase in compressive strain demand results in the development of multiple continuous crack systems and reduced strength.

Figure 2.2 also shows the typical response of plain concrete subjected to uniaxial, cyclic compression loading. Important characteristics of this response include the following:

1. Under increasing compressive strain, the stress developed follows the monotonic stress-strain response.
2. At moderate strain levels, the stiffness of the unload-reload cycles is approximately equal to the elastic modulus; however, the stiffness deteriorates with increased strain demand.

Figure 2.3 shows the normalized stress-strain response for a number of plain concrete specimens subjected to monotonic loading. Figure 2.5 and Figure 2.4 show similar

data for concrete subjected to cyclic loading. Previous research suggests that the post-peak compressive stress-strain response is dependent on specimen height, implying that compression failure is a localized phenomenon [van Mier, 1986]. The data presented in Figure 2.3 are for specimens with gage lengths that vary from 3.5 inches to 6.5 inches and this accounts somewhat for the variability of the results. The data presented in Figure 2.5 show the response of plain concrete prisms (3.0 by 5.0 by 6.5 inches) subjected to cyclic compression loading. For this configuration, it was found that peak compressive strength was approximately 85 percent of that determined using the standard compression tests. While this test program does not predict the compression strength as defined by the standardized test procedure, the results are representative of concrete subjected to cyclic compression loading.

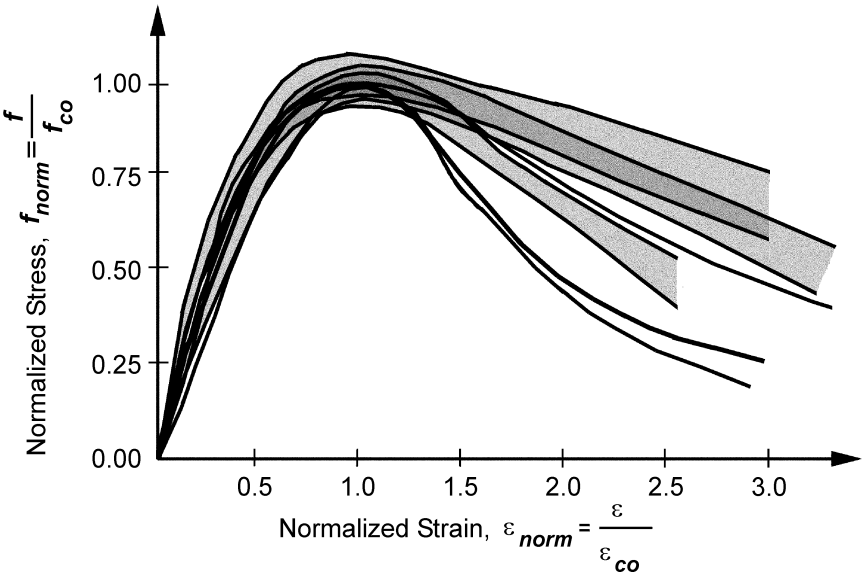

Figure 2.3: Normalized Stress-Strain Histories for Concrete Subjected to Compression Loading (Data from Bahn and Hsu [1998], Karson and Jirsa [1969], Kosaka *et al.* [1984] and Sinha *et al.* [1964])

Figure 2.6 shows a plot of normalized unloading stiffness as a function of normalized plastic compressive deformation. Plastic deformation is defined as the deformation that is not recovered upon unloading to zero compressive stress and this deformation is normalized with respect to the deformation at approximately zero compressive strength. This

applies to unload-reload cycles that occur at initial strains in excess of that corresponding to peak load. These data reflect the material damage associated with the development of continuous crack systems under severe loading. These data will be used to develop an analytical model that characterizes the deterioration of concrete stiffness under increased compressive strain demand.

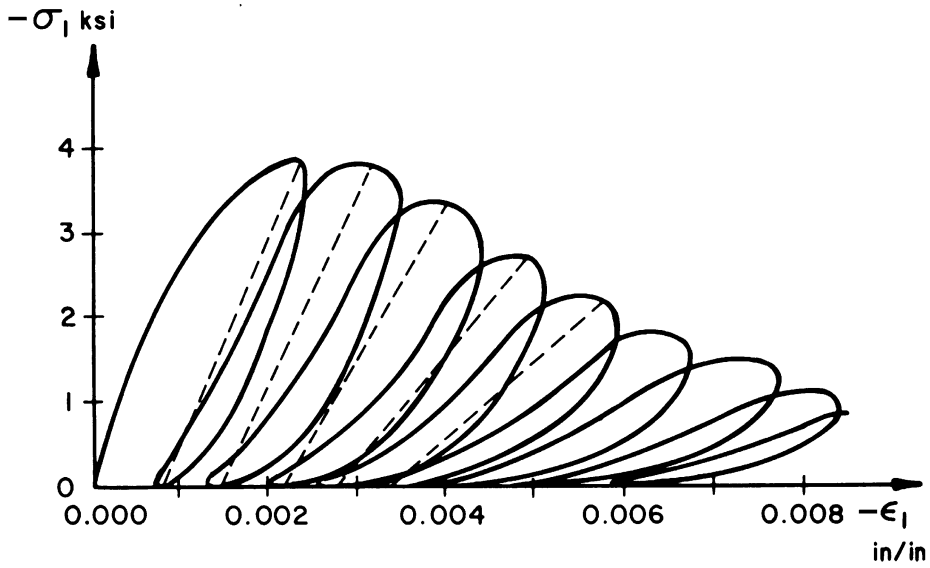

Figure 2.4: Stress-Strain History for Concrete Subjected to Uniaxial, Cyclic Compression Loading (Data from Sihna *et al.* [1964] as Presented by Chen and Han [1988])

2.2.5 Concrete Subjected to Uniaxial Tension

The response of plain concrete subjected to uniaxial tension may determine the response of reinforced concrete structural elements that are inadequately reinforced. Additionally, the deterioration of concrete tensile strength results in accelerated activation of reinforcing steel in all reinforced concrete structures. Thus, it is necessary to include representation of the deterioration of concrete tensile strength in a concrete constitutive model.

Figures 2.7, 2.8 and 2.9 show the typical stress-deformation response of plain concrete prisms subjected to uniaxial tensile deformation under monotonically increasing,

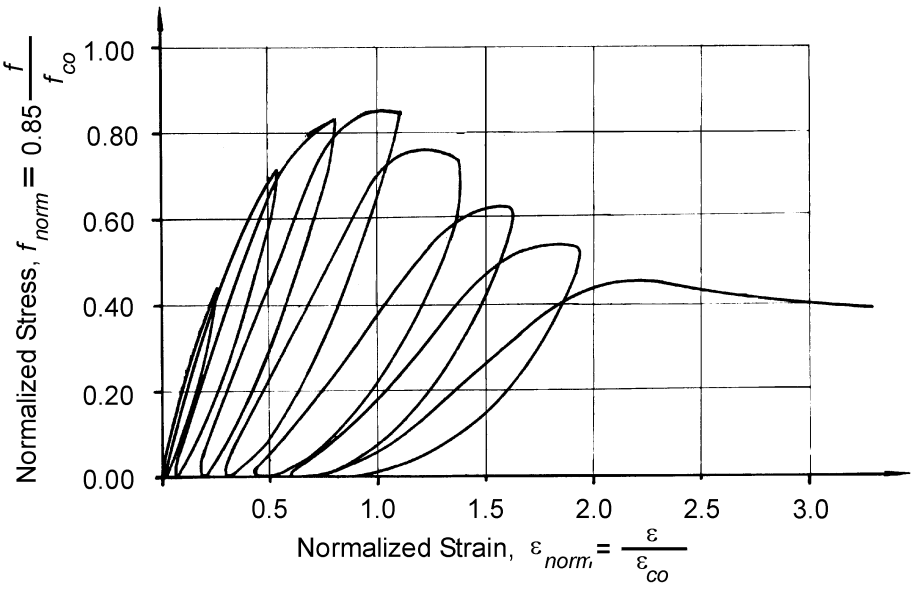

Figure 2.5: Stress-Strain History for Concrete Subjected to Uniaxial, Cyclic, Compression Loading (Data from Karson and Jirsa [1969])

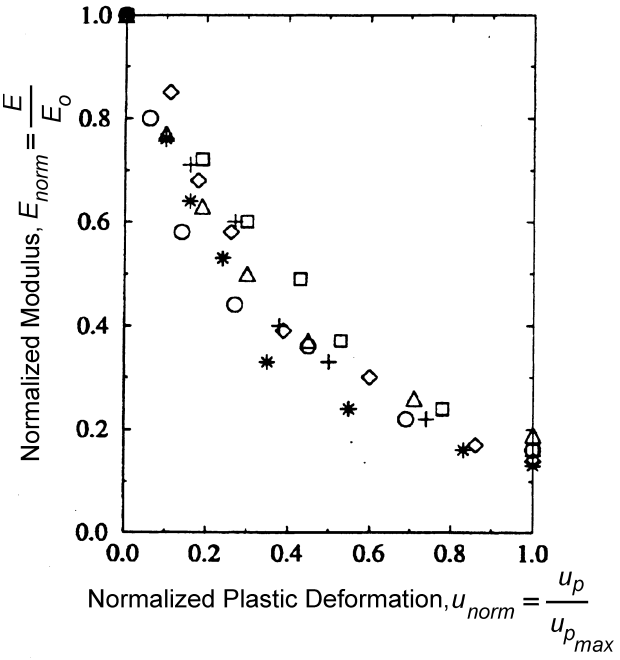

Figure 2.6: Normalized Stiffness versus Normalized Plastic Deformation (Data from Lee and Willam, 1997)

loading, cyclic loading and reversed cyclic loading. The response of plain concrete in tension is characterized by initiation, opening and propagation of cracks, thus it is inappropriate to consider tensile strain, since strain measurement depends entirely on the gage length

associated with the investigation. Important characteristics of these material responses include the following:

1. Concrete responds in an essentially linear-elastic manner until the tensile strength is achieved. This response corresponds to the initiation of a small number of stable microcracks within the transition zone.
2. Loading of the concrete to tensile strains in excess of that corresponding to the peak tensile strength results in loss of load capacity. This response corresponds to the development of continuous crack systems in the transition zone and the *hcp*.
3. Unload-reload cycles that initiate at strains in excess of that corresponding to the peak tensile strength occur at a material stiffness that is significantly less than the original material modulus. This reduced material stiffness is a result of cracks that formed under peak tensile load remaining open as long as the prism is carrying tensile stress.

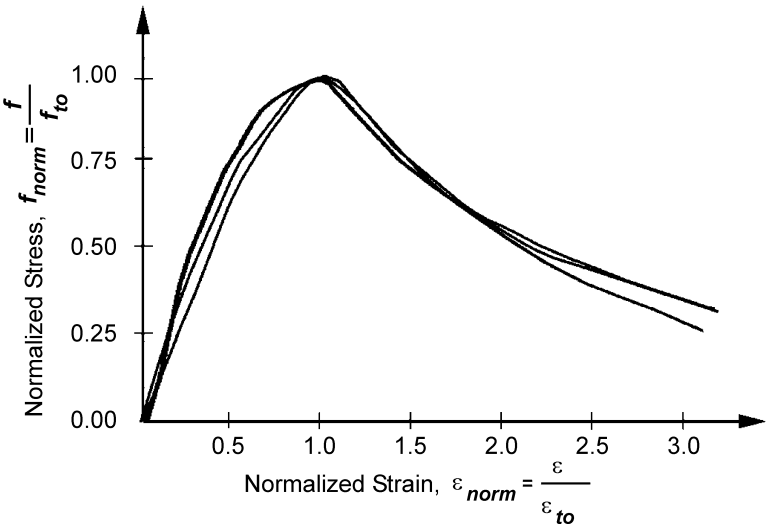

Figure 2.7: Tensile Monotonic Concrete Tensile Stress-Strain History (Data from Yankelevsky, 1987)

2.2.6 Concrete Subjected to Shear

Plain concrete subjected to monotonically increasing shear will exhibit tensile cracking perpendicular to the orientation of the principal tensile stress. In this case, material behavior may be predicted on the basis of the established concrete response to tensile

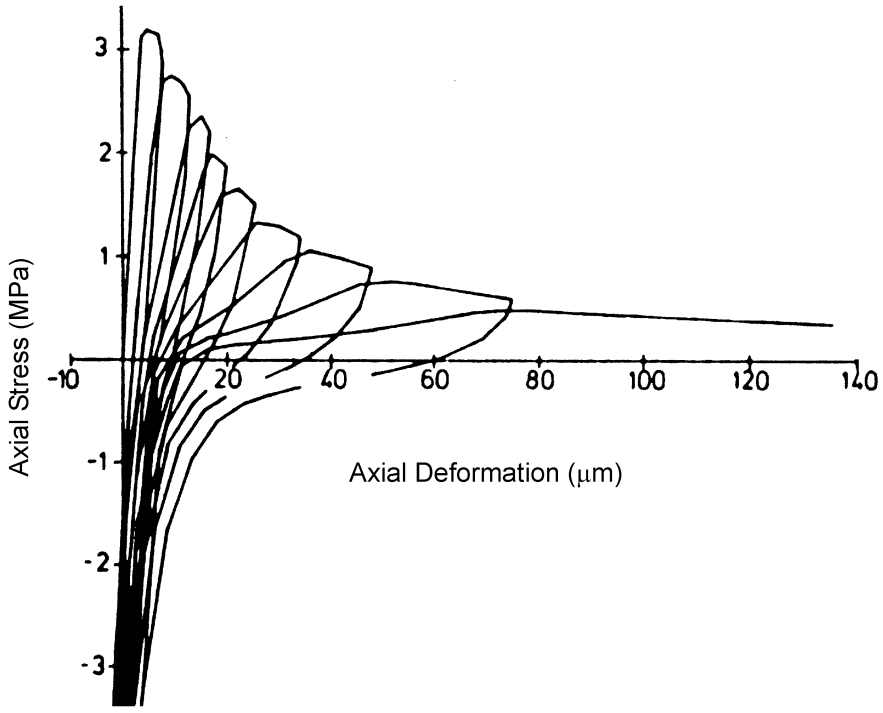

Figure 2.9: Stress-Deformation History for Concrete Subjected to Reversed Cyclic Loading (Data from Reinhardt, 1984)

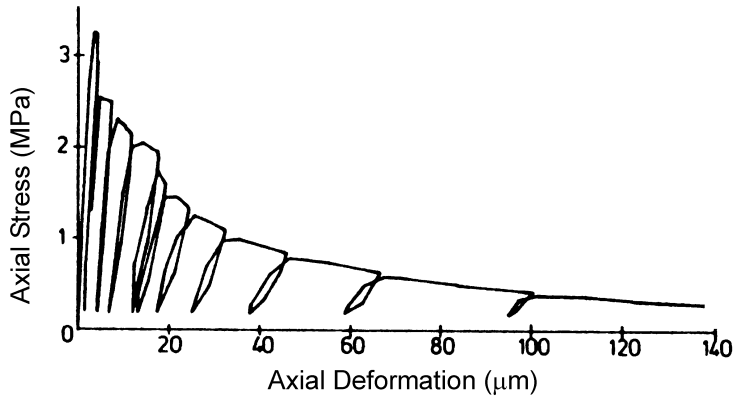

Figure 2.8: Stress-Deformation History for Concrete Subjected to Cyclic Tensile Loading (Data from Reinhardt, 1984)

loading. This implies that shear load and material response most appropriately is modeled on the basis of the combined compression and tension stress state. However, in a reinforced concrete system subjected to a general load history, regions of plain concrete may be subjected to shear loading along previously formed crack surfaces. This mechanism of

response is distinct from the response of a continuum subjected to multi-dimensional tension and compression loading. Thus, it is necessary to consider the capacity for shear transfer across a cracked concrete surface.

Shear transfer in cracked concrete has been the subject of many previous experimental investigations. Typically these investigations utilize a specimen shape that allows for the application of shear load along a well-defined cross section. Of interest to this investigation are the studies in which laboratory specimens are pre-cracked (along the appropriate cross section) under one load distribution and then subjected to shear load across the established crack surface. Also of interest to this study are the investigations in which the presence of reinforcing steel outside of the crack zone isolates concrete damage to the initial crack zone. For relatively small crack widths, load transfer across the crack plane is achieved primarily through *aggregate interlock*, the development of bearing forces between pieces of aggregate. Given this mechanism of load transfer, it is reasonable that the capacity of the system is determined by the width of the crack opening. Of particular interest to this investigation are studies in which a constant crack opening width is controlled. However, consideration of the behavior of systems in which reinforcement crossing the crack plane allows for increasing but moderate crack width is also appropriate.

Results of a few particular investigations provide insight into shear transfer in cracked concrete. An investigation conducted by Paulay and Loeber [1977] considers shear transfer in reinforced concrete specimens with pre-cracked, unreinforced, constant-width crack zones. The results of this investigation show that for small crack widths the shear stress versus slip relationship is linear to peak strength of approximately $0.20f_c$. For increased crack width, the shear stress versus slip exhibits some loss of stiffness at low load levels, but maintains a peak capacity of approximately $0.20f_c$. Results of an investigation presented by Laible *et al.* [1977] shows low shear transfer capacity ($0.06f_c$ to $0.09f_c$)

for larger crack widths (greater than 0.03 inches [0.8 mm]). Hofbeck *et al.* [1969], on the basis of an investigation of shear transfer across reinforced crack planes, propose that shear strength and stiffness increase with increasing volume of reinforcement crossing the crack plane and that the peak strength of the system is limited to $0.30f_c$. The results of this study also show that for systems in which crack width is controlled by the tensile response of steel reinforcement crossing the crack plane, the shear stress versus slip relationship exhibits deteriorating stiffness up to the peak load and then softening. This behavior may be attributed to increased crack width up to peak capacity. It is important to note that for these systems in which reinforcement crosses the crack plane, the direct contribution of steel reinforcement to shear capacity and stiffness (*dowel action*) is minimal at moderate slip levels. Similar results for systems in which steel reinforcement crosses the crack plane are presented by Walraven and Reinhardt [1981]. Here peak shear strength, achieved with high volumes of reinforcement crossing the crack plane, varies between $0.26f_c$ and $0.32f_c$.

The results of these investigations are summarized for use in developing and calibrating a concrete material model:

1. The capacity for shear transfer across a concrete crack plane as well as the stiffness of the shear stress versus slip relationship increases with increasing concrete strength and decreases with increasing crack width.
2. Concrete aggregate size and shape have relatively little effect on shear strength and stiffness.
3. Typically, under monotonically increasing slip across the crack plane, shear resistance increases up to a maximum strength of approximately $0.20f_c$ to $0.30f_c$ and then begins to decrease.

2.2.7 Concrete Subjected to Multi-Dimensional Loading

Since plain concrete in a reinforced concrete element is subjected to multi-dimensional loading, it is not sufficient to develop a constitutive model for concrete that is cali-

brated solely on the basis of the uniaxial response. A number of researchers have investigated the response of concrete subjected to two- and three-dimensional loading. Results of these investigations include analytical models characterizing the multi-dimensional compressive yield/failure surface and the evolution of this yield surface under increased loading as well as experimental data defining the concrete strain history under multi-axial loading.

2.2.7.1 Concrete Strength under Multi-Dimensional Loading

Kupfer *et al.* [1969] completed a series of tests to investigate the response of plain concrete subjected to two-dimensional loading. Yin *et al.* [1989] completed a similar investigation. In these investigations concrete plates (approximately 200 mm by 200 mm by 50 mm in dimension) were loaded to failure at prescribed ratios of σ_1:σ_2 with σ_3 equal to zero (where σ_i is the *ith* principal stress). Loads were applied using steel brushes to minimize stresses introduced through friction at the specimen boundaries. The failure surfaces developed through these investigations are presented in Figure 2.10. The result of the investigation conducted by Yin *et al.* show a failure surface that is slightly stronger than that developed by Kupfer. The difference in the failure surfaces may be due to a number of factors including load rate, conditions of the specimens during testing, preparation of the specimens, properties of the mixes or size effects. Yin *et al.* propose that the discrepancies are due in part to differences in the type of coarse aggregate used in the two studies and in part to the use by Kupfer of a slower rate of loading than is currently standard.

These two-dimensional failure surfaces are extended by data presented by Van Mier [1986] (see Figure 2.10). Van Mier investigated the effect on the two-dimensional concrete failure surface of applying low levels of confining pressure in the third dimension. Two series of tests were completed in which concrete specimens were loaded at prescribed

ratios of σ_1:σ_2:σ_3, with the stress in the one out-of-plane direction maintained at 5 or 10 percent of one of the in-plane stresses. The results of these tests show that a relatively small confining pressure in the out-of-plane reaction can significantly increase the strength of concrete in the plane of the primary loading.

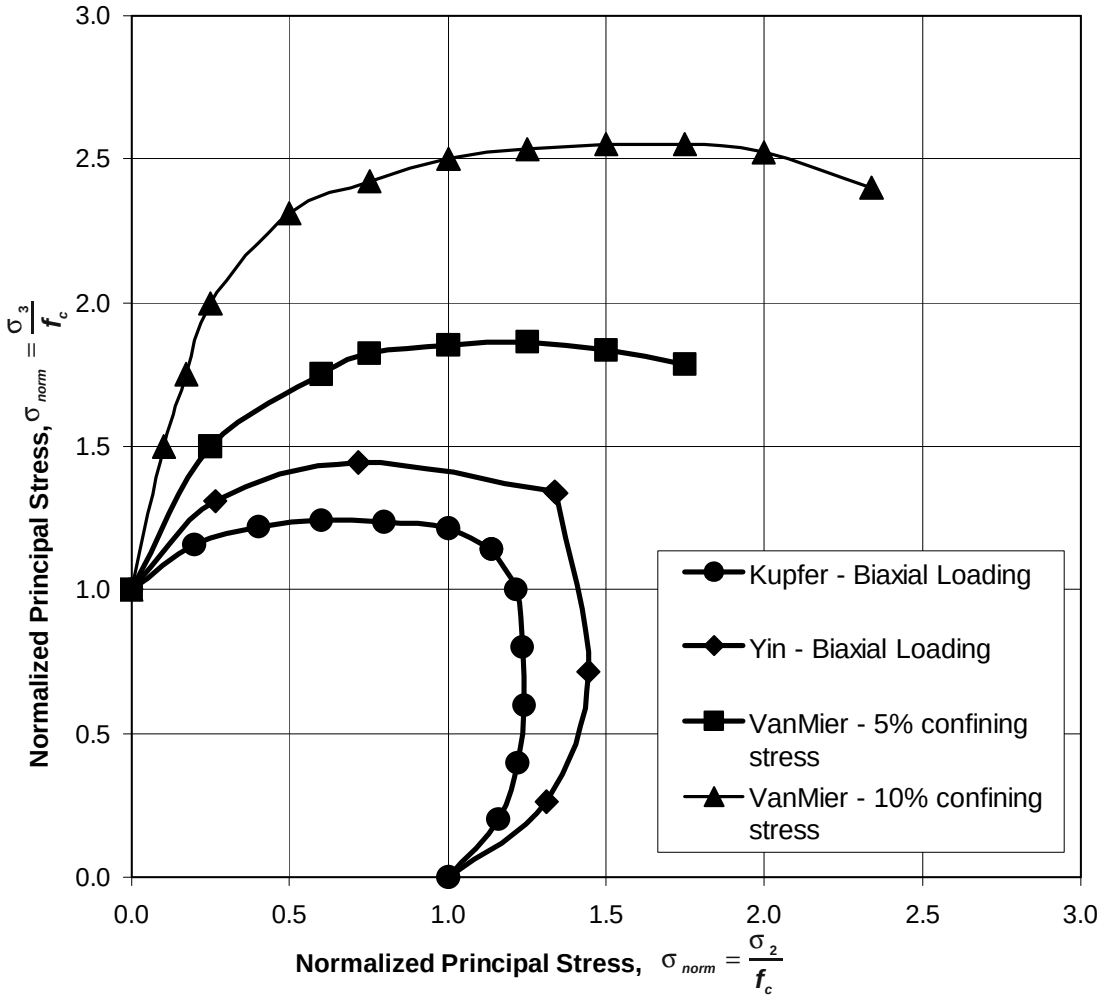

Figure 2.10:Biaxial Compressive Yield Surface for Concrete with Low Confining Pressure (Data from Kupfer *et al.* [1969], Yin *et al.* [1989] and Van Mier [1986])

The results of these two- and three-dimensional studies can be compared with results of other investigations of the response of concrete subjected to three-dimensional load histories. Figure 2.11 shows a plot of $\sqrt{J_2}$ versus I_1 where J_2 is the second invariant of the deviatoric stress tensor and I_1 is the first invariant of the stress tensor defined by the following relationships:

$$J_2 = \frac{1}{2} s_{ij} s_{ij}$$
$$= \frac{1}{6}\left[(\sigma_1 - \sigma_2)^2 + (\sigma_2 - \sigma_3)^2 + (\sigma_3 - \sigma_1)^2\right] \quad (2\text{-}6)$$

$$I_1 = \sigma_1 + \sigma_2 + \sigma_3 \quad (2\text{-}7)$$

where s_{ij} are the deviatoric components of the stress tensor defined as follows:

$$s_{ij} = \sigma_{ij} - \frac{1}{3}\sigma_{mm}\delta_{ij} \quad (2\text{-}8)$$

and δ is the Kroneker delta (Einstein summation notation convention is assumed).

In Figure 2.11 data collected from experimental investigations completed by Kosaka *et al*. [1984], Salami *et al.* [1990], and Imran *et al.* [1996] are presented in addition to the previously discussed data. The Kosaka study looks at the response of concrete loaded to failure in compression along one axis while subjected to relatively low levels of confining pressure in the perpendicular plane. For this study, the confining pressure was applied first in one plane and then the specimens were loaded to failure in compression along the perpendicular axis. Lateral confining pressure was maintained manually during the test and data show some increase as testing progressed. The presented lateral confining loads correspond to peak compressive strength. Friction along the specimen boundaries was reduced by placing greased pads between the specimen and loading frame. In the Salami and Imran studies, the initial load sequence consisted of applying an increasing hydrostatic pressure up to a specified level. Following application of hydrostatic pressure, the specimens were loaded to failure along one of the following load paths: maintain the applied pressure in two directions and increase load in the third direction, alternate a relatively large load increase in one direction with smaller load increases in the other two directions, alternate load increase in one direction with load reduction in the other two directions or simultaneously vary the load in one direction and the load in the remaining

two directions at some prescribed ratio. As with the two-dimensional testing, boundary conditions minimized frictional loads on the specimens.

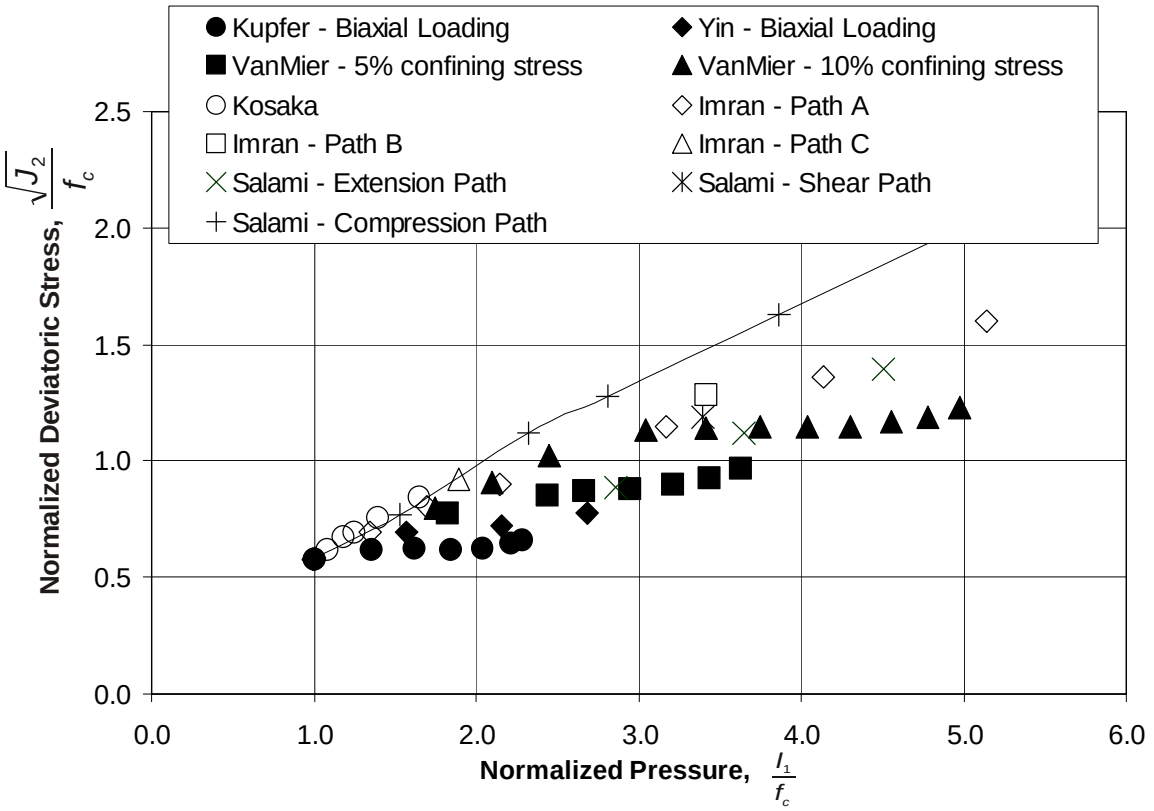

Figure 2.11:Deviatoric Stress versus Pressure at Concrete Compressive Strength

The data presented in Figure 2.11 indicate several characteristics of the concrete compressive failure surface. First, the data show that concrete subject to moderate levels of confining pressure along two principal stress axes can exhibit tremendous compressive strength along a third principal stress axis. Also, the data show that the failure surface is a function of $\sqrt{J_2}$ and I_1. However, the data show that the failure surface for concrete subjected to general three-dimensional loading is not uniquely defined by $\sqrt{J_2}$ and I_1. Instead, the data presented in Figure 2.11 indicate that the relationship between $\sqrt{J_2}$ and I_1 is a function of the ratio of the principal stresses. This is evident in the comparison of the data presented by Kupfer *et al.*, Yin *et al.* and Van Mier with that presented by Salami. Within each of the first four data sets, most of the data points represent approximately the

same loading in two dimensions and variable loading in the third dimension. For example, most of the data points in the data set presented by Van Mier for 5 percent confinement stress represent a stress state in which $\sigma_3 \cong 1.80 f_c$, $\sigma_1 = 0.05\sigma_3$ and $0.6 f_c > \sigma_2 > 1.75 f_c$. On the other hand, the data presented by Salami for compressive loading represents stress states in which the ratio between the principal stresses is approximately constant and thus the confining pressure in two dimensions varies with the compressive strength achieved in the third dimension. The non-uniqueness of the $\sqrt{J_2}$ and I_1 relationship is further supported by the data presented in Figure 2.12. Here the data indicate that there is a linear relationship between minimum and maximum normalized principal stress at peak compressive load.

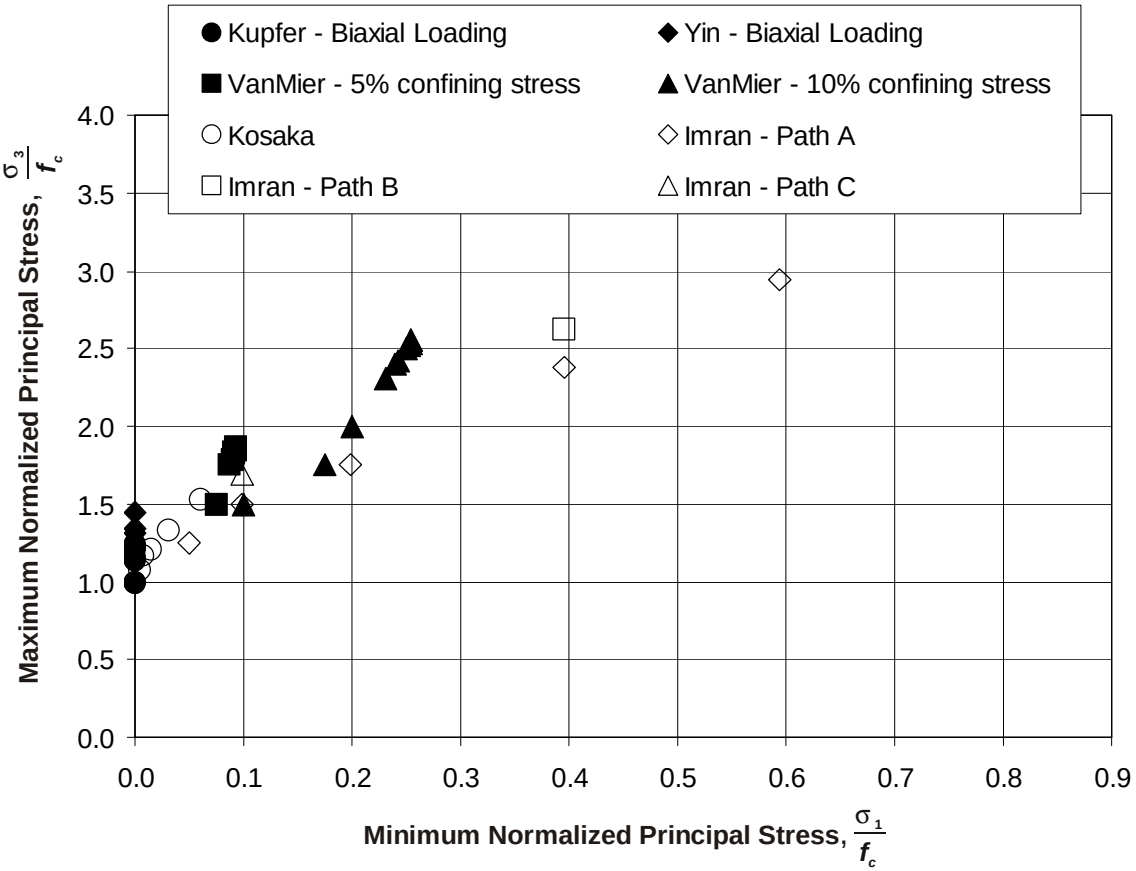

Figure 2.12:Maximum Versus Minimum Normalized Principal Stress (Data from Sources Identified in Figure 2.11)

2.2.7.2 Evolution of the Yield Surface Under Multi-Dimensional Loading

There are few investigations that have considered the evolution of the concrete multi-dimensional yield surface from the initial inelastic response through complete loss of strength. A thorough investigation of the topic requires a coordinated effort between experimental and analytical research since the evolution is unique to the plasticity model. Kupfer *et al.* [1969] propose that the shape of the biaxial yield surface for concrete loaded in compression maintains the same shape throughout the loading process. Lubliner *et al.* [1989] propose that the limit of the elastic domain for concrete loaded in multi-dimensions appropriately is defined on the basis of the uniaxial stress-strain response. Conversely, Salami and Desai [1990] propose some moderate modification to the yield surface for concrete loaded in three dimensions. The most extreme variation in the concrete yield surface is that proposed by Chen and Han [1988]. In this model, the researchers propose a model that is consistent with experimental observation that while the initial elastic domain excludes extreme loading of concrete in hydrostatic pressure, the ultimate yield surface does not.

2.2.7.3 Concrete Strain History Under Multi-Dimensional Loading

In experimental investigations concrete exhibits variation in volumetric strain as a function of deviatoric stress. This dilatant response is revealed explicitly in the data presented by Stankowski and Gerstle [1985] (Figure 2.13). However, concrete dilatancy is also revealed in the more commonly presented volumetric strain versus compression load for concrete tested in uniaxial compression (Figure 2.14). Here dilatancy contributes to the volumetric expansion observed near peak load capacity. In reinforced concrete structural elements, volumetric expansion activates transverse reinforcement and thus may determine the mechanism of response. This characteristic of concrete response properly is considered in development of a concrete material model.

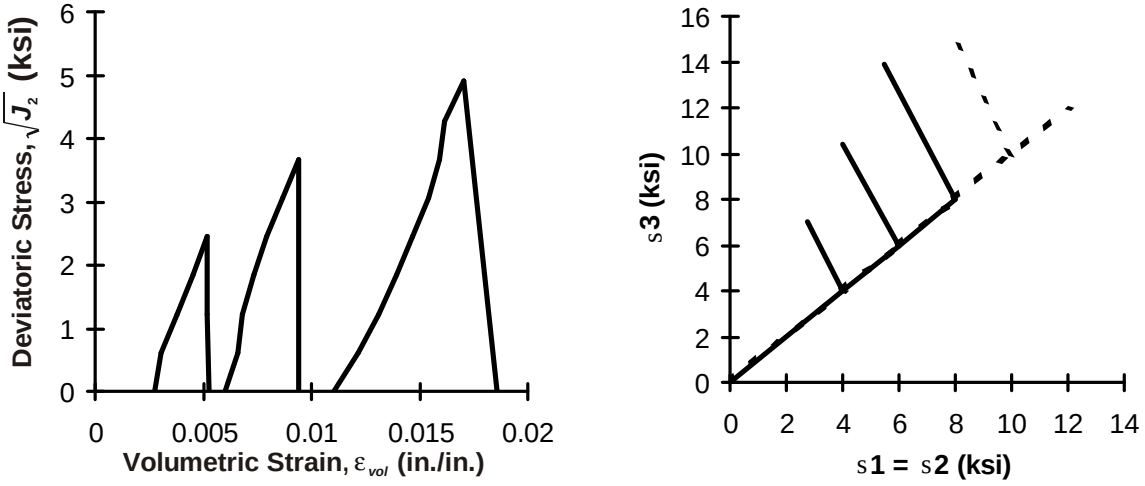

Figure 2.13:Deviatoric Stress Versus Volumetric Strain (Data from Stankowski and Gerstle [1985])

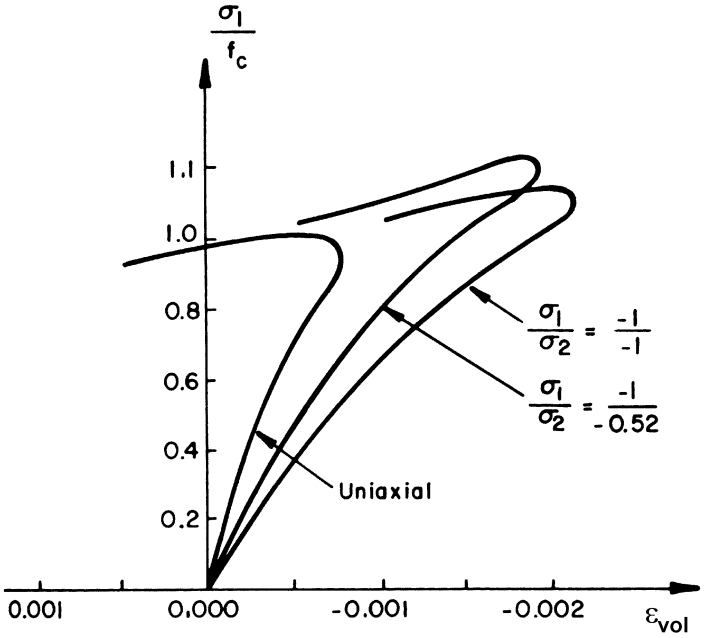

Figure 2.14:Concrete Compressive Stress Versus Volumetric Strain (Data from Kupfer, 1969 as Presented by Chan and Han, 1988)

2.2.8 The Effect of Load Rate on Concrete Response

Time represents the fourth dimension for concrete loading, and a number of researchers have investigated the effect of load rate on concrete material response. Since the focus of this study is the analysis of reinforced concrete members subjected to earthquake load-

ing, it is necessary to consider the response of concrete subjected to the moderately rapid load rates associated with earthquake ground motions.

Load rate for materials is most appropriately considered in terms of applied strain rate. Numerical modeling [*e.g.,* Wakabayashi *et al*., 1984] and experimental, dynamic testing of full-scaled models [*e.g.,* Hosoya *et al.,* 1997] has been used to investigate the strain rate associated with earthquake loading of reinforced concrete structures. This research indicates that the strain rate is a function of the period of the structure, the earthquake ground motion and the ductility demand on the structural elements. This research and the investigations of others [Mahin and Bertero, 1972] identify the maximum strain rate in reinforced concrete structures subjected to severe earthquake ground motion to be between 0.001 per second and 0.25 per second.

An appropriate range for maximum strain-rates for plain concrete in a bridge frame subjected to earthquake loading can be estimated on the basis of the typical period range for these structures. Here we will assume that the period, T_{bridge}, is not the purely elastic period but includes some softening of the system due to cracking of concrete under service level and environmental loading. For the case of a brittle failure of a bridge connection due to overloading of plain concrete in tension, it is reasonable to assume that maximum tensile strength will be reached at the point of maximum displacement. This will correspond to loading during an time interval equal to $0.25T_{bridge}$. A plausible range for the period of a reinforced concrete bridge is 0.25 sec. to 1.0 sec. Thus, concrete strength is assumed to be achieved during a minimum time interval of 0.0625 sec. For average-weight, normal-strength concrete, tensile strength is achieved at a strain of approximately 10^{-4}. This implies a maximum strain rate of approximately 0.002 per second.

An appropriate maximum strain-rate for the case of crushing of plain concrete, is estimated assuming that crushing occurs once some inelastic deformation has occurred in

the bridge. For this case, peak flexural demand is assumed to developed during a load increment equal to $0.25T_{yield}$. Here T_{yield} defines the effective period of the bridge for the case of some inelastic deformation. A reasonable estimate for T_{yield} is $2T_{bridge}$ assuming an average ductility demand of 4. The compressive strain corresponding to crushing of plain concrete is approximately 0.006 for average-weight, normal-strength concrete. On the basis of these assumptions, it follows that a maximum strain rate for consideration of concrete crushing strength is 0.05 per second.

In considering the effect of load rate of concrete response it is appropriate to consider variation in compressive and tensile strength and material stiffness. Additionally, since concrete material response is controlled by damage mechanism, it is necessary to consider the effect of load rate on concrete fracture energy.

A number of researchers have investigated the response of concrete subjected to loading at strain rates up to 10 percent strain per second. Material testing at these strain rates requires an experimental test set-up in which it is possible to record data at very high rates and for which it is possible to determine the loads applied to the test specimen as well as the loads transferred back into the test frame.

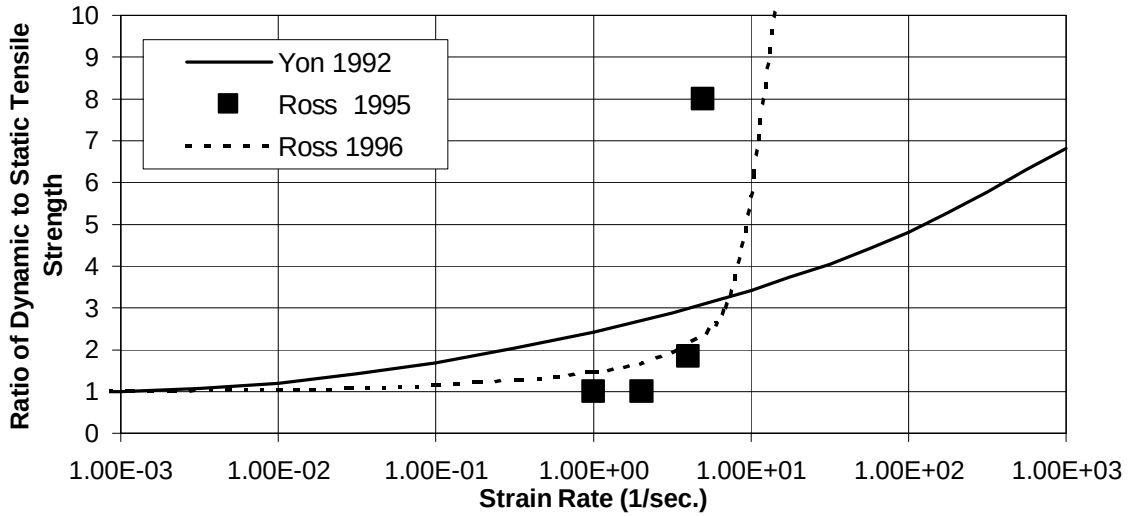

Figure 2.15:Effect of Strain Rate on Concrete Tensile Strength

Figure 2.15 shows two proposed relationships between the dynamic to static tensile strength ratio and strain rate, as well as additional experimental data. The relationship proposed by Ross *et al.* [1996] is derived on the basis of fracture mechanics and calibrated to fit experimental data provided by the authors and by Ross *et al.* [1995]. The relationship proposed by Yon [1992] is developed to fit empirical data. The data provided by Ross [1995, 1996] follow from dynamic split-cylinder testing of 51 mm-diameter by 51 mm-long (2.0 by 2.0 inches) concrete specimens that were cut from 300 mm square concrete cubes (12 inch cube). Yon determined concrete tensile strength from three point bending tests of 16.0 by 3.75 by 2.00 inch (407 by 95.4 by 50.9 mm) plain concrete beams. The data presented in Figure 2.15 indicate that for the strain rates of interest to this investigation, there is an increase in tensile strength over the static strength. The extent of this increase varies for the different experimental data sets. However, at these strain rates, the increased strength is not as significant as is found for strain rates in excess of 100 percent per second.

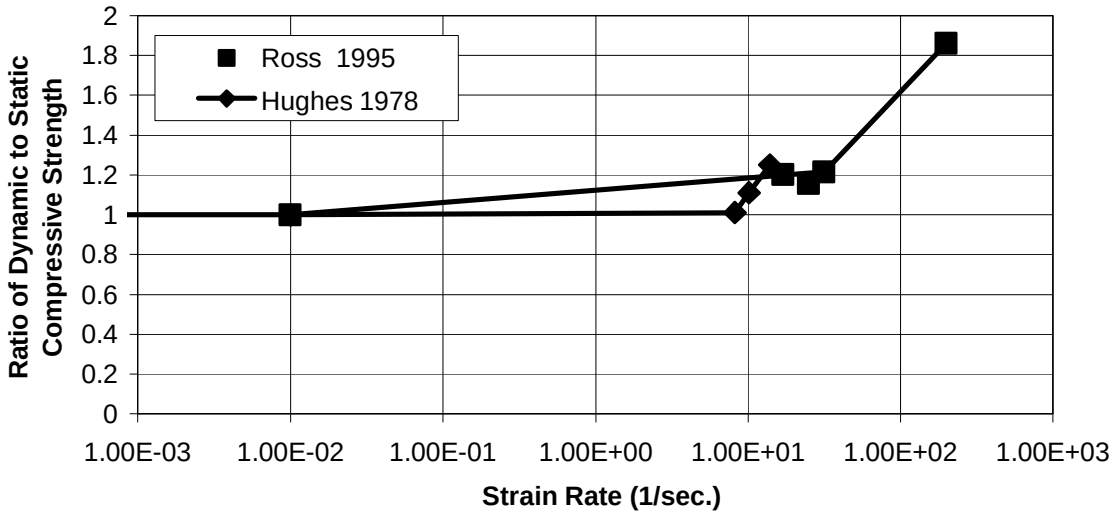

Figure 2.16:Effect of Strain Rate on Concrete Compressive Strength

Figure 2.16 shows two proposed relationships between the dynamic to static compressive strength ratio and strain rate. The relationship proposed by Ross *et al.* [1995] fol-

lows from material testing of the 51 mm-diameter by 51 mm-long (2 inch by 2 inch) concrete specimens in compression. The authors note that the compression specimens fail through the development of cracks along the axis of loading, apparently indicating that the compressive strength is actually determined by the tensile strength in the direction perpendicular to the applied loading. The data provided by Hughes and Gregory [1978] is from impact tests in which a steel hammer was dropped on 102 mm (4.01 inch) concrete cubes. For the compression specimens, the transition between dynamic and static response occurs at a strain rate of approximately 10.0 per second, Ross *et al.* [1996] note that this correlates with their proposed relationship for dynamic concrete tensile strength. The data appear to indicate that the compressive strength increases at most 10 to 15 percent within the strain rate in the range of interest to this study. This correlates well with experimental testing of reinforced concrete specimens in which the nominal strength of the members increases by approximately 10 percent under dynamic loading [Hosoya, 1997].

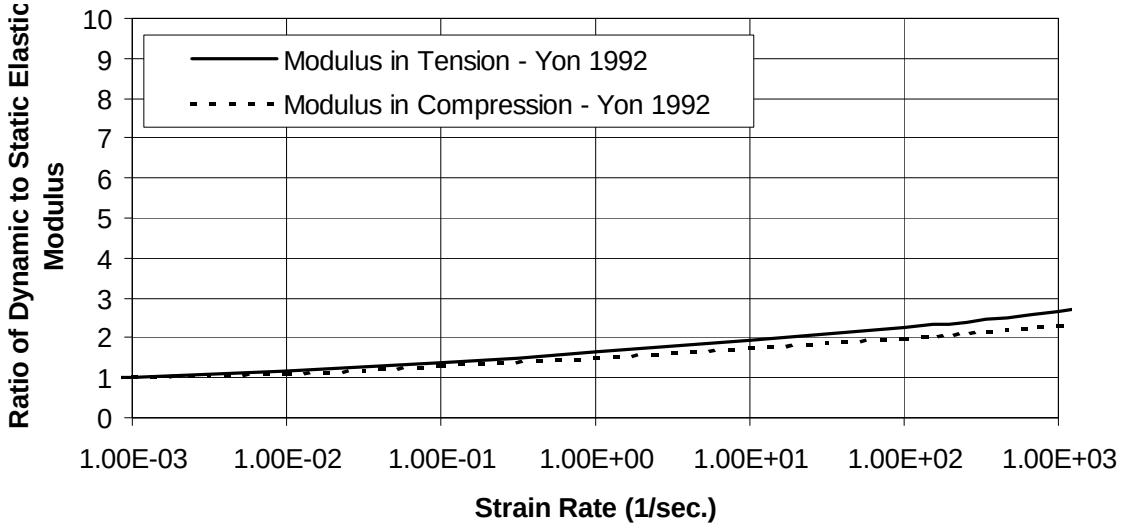

Figure 2.17:The Effect of Strain Rate on Concrete Elastic Modulus

The experimental investigations also considered the effect of strain rate on various other concrete material parameters including elastic modulus and fracture energy. All conclude that concrete fracture energy is independent of strain rate. Additionally, with the

exception of Yon, all of the presented investigations consider elastic modulus to be independent of strain rate. Yon does propose a relationship in which there is an increase in elastic modulus within the strain rate of interest to this study (Figure 2.17).

2.2.9 Concluding Remarks About Concrete Material Properties

The previous sections present data that characterize the response of plain concrete to various specific load histories. The data indicate that this response is characterized in part by a number of material parameters including uniaxial compressive strength, uniaxial tensile strength, elastic modulus, poison ratio and fracture energy. Additionally, the data show that the concrete response is determined by damage mechanisms that are reflected in reduced material modulus following severe loading as well as by plastic mechanisms that are reflected in accumulated, unrecoverable plastic strain upon unloading. The data show that the concrete response is a function of the multi-dimensional stress-state, the load history, and the rate of loading.

Experimental data also show significant variability in measured response. This variability results in part from variation in the test set-up and procedure utilized by various researchers. However, this variability is also a result of variation in testing conditions (*e.g.*, temperature and humidity) and concrete component properties (*e.g.*, cement, sand, aggregate and add mixtures) that cannot explicitly be incorporated into a material model because of insufficient data. This variation in experimental data suggests that an appropriate concrete constitutive model predicts the fundamental characteristics of concrete response rather than the results of specific experimental test programs.

Finally, the experimental data suggest that a highly sophisticated analytical model is required to characterize concrete response under all possible load histories. Such a model may be impractical and computationally infeasible. For this reason, Gerstle *et al.* [1980] propose that the simplicity of the model should be considered in addition to the accuracy

of model prediction. An appropriate approach for this study is to develop a constitutive model that predicts the fundamental characteristics of response within the range of loading that is expected for reinforced concrete beam-column joint subjected to earthquake loading.

2.3 Concrete Constitutive Models

In recent years there has been a tremendous effort aimed at developing analytical models that accurately predict the response of plain concrete to variable loading. Early models relied on elasticity theory. More recently proposed models utilize general theories of solid mechanics including plasticity theory, damage theory and fracture mechanics.

The majority of these proposed models predict particular aspects of concrete response with an acceptable level of accuracy and efficiency. However, in considering these models as a first step toward development of a constitutive model for this particular investigation, it is necessary to consider a number of particular issues including the following:

- Evolution of the failure surface for both one-dimensional and multi-dimensional loading and particularly for two-dimensional loading with minimal confining pressure in the third dimension.
- Representation of material damage exhibited under both compression and tension loading.
- The manner in which softening is incorporated and calibrated.
- Dilatancy associated with compressive failure.
- Representation of concrete shear response.
- Representation of loading from compression into tension and the reverse.

2.3.1 Elasticity Theory Applied to Modeling Concrete Behavior

Some of the first proposed constitutive models were developed on the basis of elasticity theory and utilized a variety of methods to represent the non-linear response of con-

crete under multi-dimensional, reversed-cyclic loading. One approach was to follow a Hookean formulation with non-linear functions representing the concrete material response:

$$\sigma_{ij} = F_{ij}(\varepsilon_{kl}) \tag{2-8a}$$

$$\sigma_{ij} = D^{s}_{ijkl}(\sigma_{pq})\varepsilon_{kl} \tag{2-8b}$$

Here D^{s}_{ijkl} defines the secant material stiffness. This approach is suggest by Ahmed and Shah [1982]:

Such a model may be used to represent the response of concrete subjected to moderate loading. However, because this model implies a one-to-one correspondence between stress and strain, such a model is not appropriate for predicting the response of concrete subjected to severe loading in which case load reversals and monotonic loading past peak result in multiple strain states being associated with a single stress state.

A second approach is to characterize the tangent material stiffness and to define the stress and strain states incrementally:

$$\dot{\sigma}_{ij} = D^{t}_{ijkl}(\sigma_{pq},\varepsilon_{kl})\dot{\varepsilon}_{kl} \tag{2-9}$$

Here D^{t}_{ijkl} defines the tangent material stiffnesses. This approach is presented by Gerstle [1981].

Such an approach can be used to characterize the response of concrete subjected to variable load histories. However, without additional criteria, determining appropriate values for the tangent material stiffness may not be practical.

2.3.2 Plasticity Theory Applied to Modeling Concrete Behavior

The defining characteristic of material plasticity is the accumulation of unrecoverable deformation upon loading beyond the yield limit. The previously presented data show

that concrete exhibits this characteristic when loaded in compression and, to a lesser extent, when load in tension (see Figures 2.3, 2.5, 2.8 and 2.9). Thus, it is appropriate that a constitutive model for plain concrete incorporate plasticity theory.

Development of a plasticity-based constitutive model requires defining a rule for decomposition of the total strain, the elastic material constitutive relationship, the yield/ failure surfaces that bound the elastic domain and the flow rules that define the evolution of the internal variables. Traditionally, the total strain, ε, is assumed to be the sum of the elastic strain, ε^e, and the accumulated plastic strain, ε^p:

$$\varepsilon = \varepsilon^e + \varepsilon^p \tag{2-10}$$

It is reasonable to assume that concrete is a homogenous material; thus, the elastic material properties are readily defined on the basis of data collected from standard material tests and the elastic constitutive relationship follows Hooke's Law:

$$\sigma_{ij} = C_{ijkl}\varepsilon^e_{kl} \tag{2-11}$$

where C_{ijkl} is the rank four material stiffness tensor. The yield surface or surfaces bound the elastic domain. Following classical plasticity theory, the elastic domain is defined in stress space. For concrete, the available material data facilitated definition of the yield surface in stress space and it is most appropriate to consider a yield surface that evolves as a function of the load history. A hardening rule defines the evolution of the yield surface. The flow rules define the evolution of a set of internal variables that uniquely define the material state. In particular a flow rule defines the orientation of plastic strain which may be associated, defined as normal to the yield surface, or non-associate. Proposed models for concrete vary in the definition of the yield surface, the hardening rules and the flow rules.

2.3.2.1 Yield Surfaces for Concrete Plasticity Models

A variety of yield surfaces have been proposed to characterize the response of plain concrete. Two of the first were the Mohr-Coulomb (dating from 1800) and the Drucker-Prager [1952] criterion. These criteria were developed to describe the response of material such as rock, sand and concrete for which hydrostatic pressure affects the material yield and failure strengths. The Mohr-Coulomb criterion is defined as follows:

$$f(I_1, J_2, \theta) = \frac{1}{3} I_1 \sin\phi + \sqrt{J_2}\sin\left(\theta + \frac{\pi}{3}\right) + \frac{\sqrt{J_2}}{\sqrt{3}}\cos\left(\theta + \frac{\pi}{3}\right)\sin\phi - c\cos\phi \qquad (2\text{-}12)$$

In Equation (2-12) I_1 and J_2 are invariants of the stress states as previously defined, ϕ and c are material parameters and θ is also an invariant of the stress state defined as follows:

$$\theta = \frac{1}{3}\text{acos}\left(\frac{3\sqrt{3}}{2}\frac{J_3}{J_2^{3/2}}\right) \qquad (2\text{-}13)$$

where J_3 is the third invariant of the deviatoric stress, defined as follows:

$$J_3 = \frac{1}{3} s_{ij} s_{jk} s_{ki} \qquad (2\text{-}14)$$

Equations (2-12) and (2-13) represent a straight line of variable slope in the meridian plane and an irregular hexagon in the π-plane (see Figure 2.18). The Mohr-Coulomb criterion rarely is utilized in current concrete models in part because of the discontinuity of the surface hinders numerical implementation and in part because recent investigations show the Mohr-Coulomb criterion to be only a moderate fit to experimentally observed material response.

The Drucker-Prager criterion represents moderately well the response of plain concrete subjected to multi-axial compression and provides a smooth yield surface (Figure 2.18). This criterion is incorporated into some currently proposed concrete material models and is defined as follows:

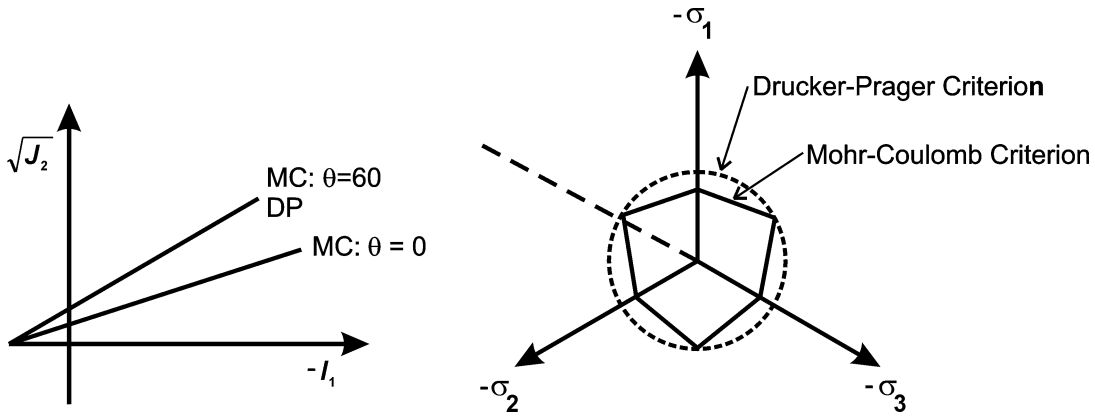

Figure 2.18:Mohr-Coulomb and Drucker-Prager Failure Criteria

$$\sqrt{J_2} + \alpha I_1 + y = 0 \tag{2-15}$$

In Equation (2-15) α and y are material parameters that in the original formulation are considered to be constant but that vary with load history in more recent implementations.

Figure 2.19 shows the Drucker-Prager criterion for several values of α and y compared with experimental data. As indicated in Figure 2.19, Imran and Pantazopoulou [1996] propose $\alpha = 0.3$ for characterizing the response of concrete subjected to triaxial compression. The response of concrete subjected to biaxial compressive loading (Kupfer *et al.* [1969] and Yin [1989]) is characterized well by $\alpha = 0.1$. All of the presented yield criteria are calibrated to predict the observed uniaxial compressive strength.

Comparison of the Drucker-Prager criterion with experimental data shows that while the criterion may be used to represent the response of concrete subjected to multi-axial compression, the model over-estimates the capacity of concrete subjected to compression-tension or tension-tension type loading. Variation in concrete response under various load regimes has been addressed by a number of researcher through the use of multi-surface plasticity models. Murray *et al.* [1979] propose a three surface model to characterize the response of plain concrete subjected to biaxial loading (Figure 2.20). This approach was extended to concrete loaded in three-dimensions by Chen and Chen [1975], and Lubliner *et al.* [1989] (see Figure 2.21). It is interesting to note that the Lubliner model uses the

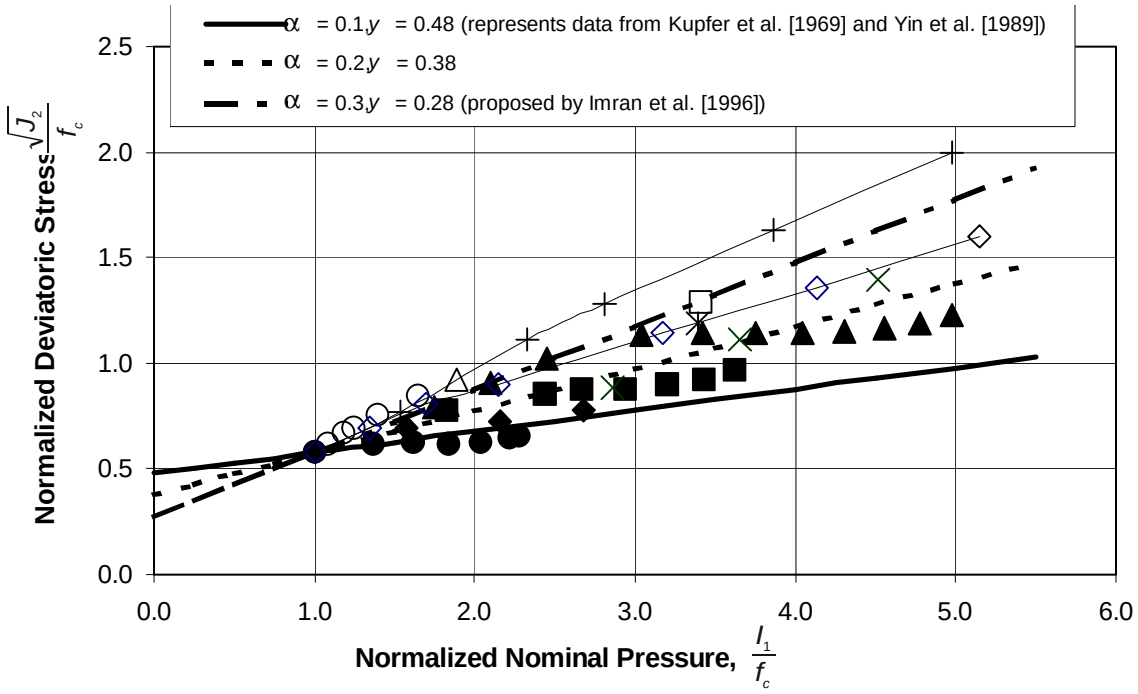

Figure 2.19:Drucker-Prager Failure Criterion Compared with Experimental Data (Data as Presented in Figure 2.11)

Drucker-Prager criterion to characterize the response of concrete subjected to triaxial compression. While the introduction of multiple, intersecting failure surfaces may facilitate definition of the entire yield surface, it may complicate determination of flow equations as will be discussed in the following paragraphs.

Data indicate that concrete subjected to severe hydrostatic pressure loading does not respond elastically as is implied by some models [*e.g.*, Drucker-Prager 1952; Murray *et al*, 1979; Vermeer *et al.*, 1984] in which the failure surface is linear in $\sqrt{J_2} - I_1$ space. This issue has been addressed in a number of models that limit the elastic range under severe hydrostatic pressure. Some of the models introduce a non-linear relationship between $\sqrt{J_2}$ and I_1 [*e.g.*, Han and Chen, 1985; and de Boer and Dresenkamp, 1989] and some actually "cap" [Drucker *et al.*, 1975; Schofield and Wroth, 1968; Sandler *et al.*, 1976] concrete capacity under hydrostatic pressure [e.g., Salami and Desai, 1990].

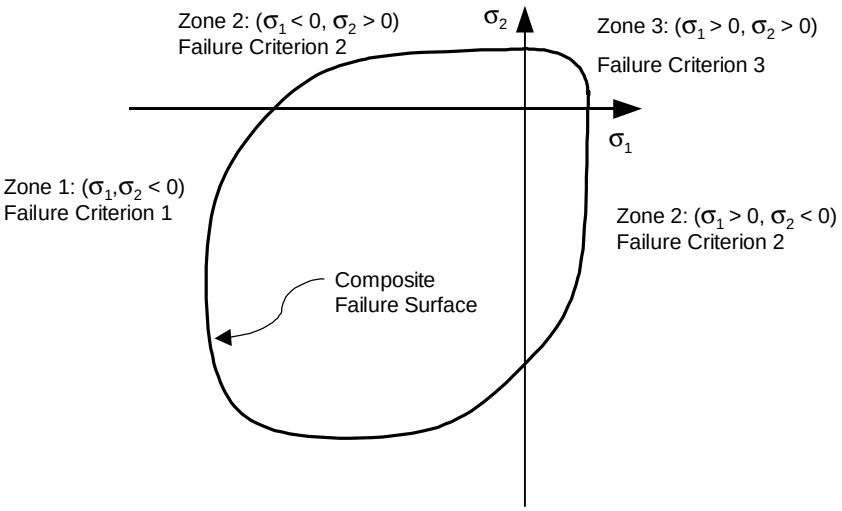

Figure 2.20:Multi-Surface Plasticity Model for Concrete Subjected to Biaxial Loading [Murray *et al.* 1979]

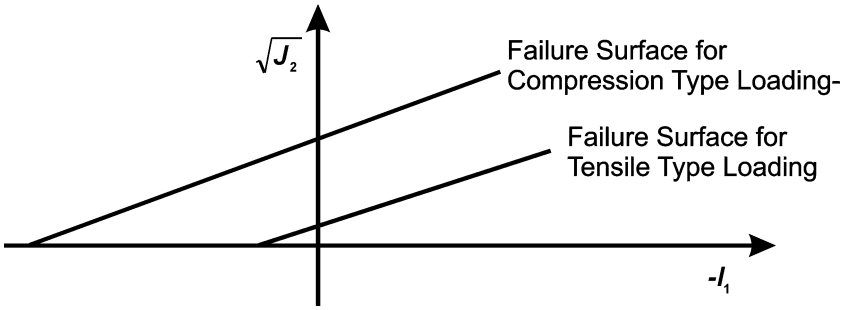

Figure 2.21:Multi-Surface Plasticity Model for Concrete Subjected to Triaxial Loading [Lubliner *et al*., 1989]

Also of interest is the evolution of the failure surface as a function of increased loading. This evolution is typically defined by a hardening rule. Some models assume that the shape of the yield surface remains the same with the elastic region expanding and contracting as a function of load history [Kupfer *et al.*, 1969; Chen and Chen,; Murray *et al.*, 1979]. In this case the hardening function is a scalar and the yield surface takes the following form:

$$f(s) = \tilde{f}(s) - y(\lambda) = 0 \tag{2-16}$$

where y defines the yield strength and λ is a function of the load history. There are few data defining the rate at which the concrete elastic domain expands and contracts under multi-axial loading, as a result it is reasonable to calibrate the hardening function on the basis of the well-defined uniaxial concrete response [Murray *et al.*, 1979; Lubliner *et al.*, 1989]. Many models account for variation in the shape of the yield surface that occurs as concrete is loaded from the point of initial inelasticity to the point of maximum load and beyond to the point of minimal capacity. Models that propose variable shaped yield surfaces include that proposed by Han and Chen [1985], Ohtani and Chen [1988], de Boer and Dresenkamp [1988], Zama *et al.* [1993]. For these models the yield surface takes the following form:

$$f(s) = \tilde{f}(s) - y(\lambda, \sigma) = 0 \tag{2-17}$$

where the hardening rule y is a function of the load history as represented by λ as well as the current stress state, σ, thereby allowing for variation in the shape of the yield surface.

The model proposed by Chen and Han [1988] incorporates many of the techniques currently used in development of a concrete yield surface that evolves under a variable load history. This model proposes that at the maximum load, the yield surface appropriately may be defined following the recommendations of any of several researchers [Ottosen, 1977; Hsieh *et al.*, 1982; Willam and Warnke, 1975]. The complete surface proposed by Ottosen [1977] is composed of two similar surfaces as follows:

$$f(I_1, J_2, \theta) = aJ_2 + \lambda\sqrt{J_2} + bI_1 - 1 = 0 \tag{2-18a}$$

where λ is a function of $cos3\theta$:

$$\lambda = \begin{cases} k_1 \cos\left[\frac{1}{3}\text{acos}(k_2 \cos 3\theta)\right] & \text{for } \cos 3\theta \geq 0 \\ k_1 \cos\left[\frac{\pi}{3} - \frac{1}{3}\text{acos}(-k_2 \cos 3\theta)\right] & \text{for } \cos 3\theta \leq 0 \end{cases} \tag{2-18b}$$

For this model, the initial elastic domain is closed (concrete subjected to hydrostatic pressure responds inelastically) and defined by the yield surface at maximum loading. For the Ottosen surface the initial yield surface is defined as follows:

$$f(\sigma) = \rho - k\rho_f = 0 \tag{2-19a}$$

where

$$\rho = \sqrt{J_2} \tag{2-19b}$$

$$\rho_f = \frac{1}{2a}[-\sqrt{2}\lambda + \sqrt{2\lambda^2 - 8a(bI_1 - 1)}] \tag{2-19c}$$

$$k = k(I_1) \tag{2-19d}$$

and where λ is a shape function that maps between the initial yield surface and the yield surface defining peak strength and is defined as in Equation (2-18b). The yield surface defined by this model is depicted qualitatively in Figure (2.22).

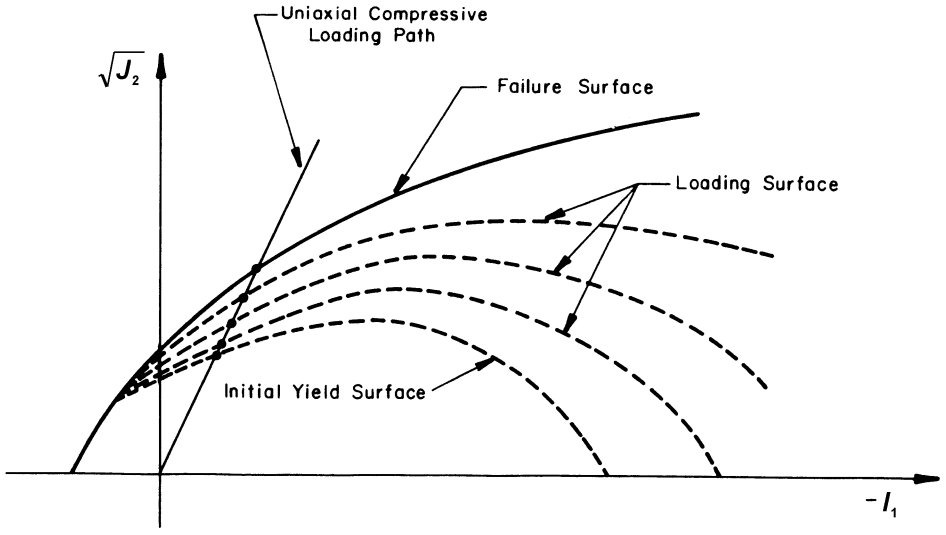

Figure 2.22:Evolution of Concrete Yield Surface as Proposed by Chen and Han [1988]

2.3.2.2 Flow Rules for Concrete Plasticity Models

Definition of a plasticity-based constitutive model requires establishing flow rules that define the evolution of a set of internal variables. Of particular interest is the plastic flow rule that defines the orientation of the plastic strain. The plastic strain rate is defined as follows:

$$\dot{\varepsilon}^p = \lambda \frac{\partial}{\partial \sigma} g(\sigma, q) \tag{2-20}$$

where $\dot{\varepsilon}^p$ is the rate of plastic strain, λ is a positive scalar, q is the set of internal variables and $g(\sigma, q)$ is the plastic potential function. Typically it is assumed that the orientation of plastic flow is normal to the yield surface in which case the plastic potential function is the yield function. Following this assumption of *associated flow* the increment of plastic strain is defined as follows:

$$\dot{\varepsilon}^p = \lambda \frac{\partial}{\partial \sigma} f(\sigma, q) \tag{2-21}$$

It has been shown that the assumption of associated flow assures a unique solution for a given boundary-value problem in which the material stress-strain relationship is perfectly plastic or exhibits work hardening[1]. Additionally, this assumption results in a symmetric algorithmic tangent that greatly enhances the efficiency of numerical solution methods. Thus, the assumption of associated flow is both theoretically and numerically desirable. A number of plasticity models have been developed assuming associated flow [*e.g.*, Ohtani and Chen, 1988; Salami, 1990]. These models characterize moderately well the response of concrete over a range of load histories (Figure 2.23).

Experimental data, however, indicate that associated flow may not be the most appropriate assumption for characterizing the response of concrete. Researchers have noted that concrete displays shear dilatancy characterized by volume change associated

1. A discussion of uniquenss theorems applied to plasticity theory is provided by Lubliner [1990].

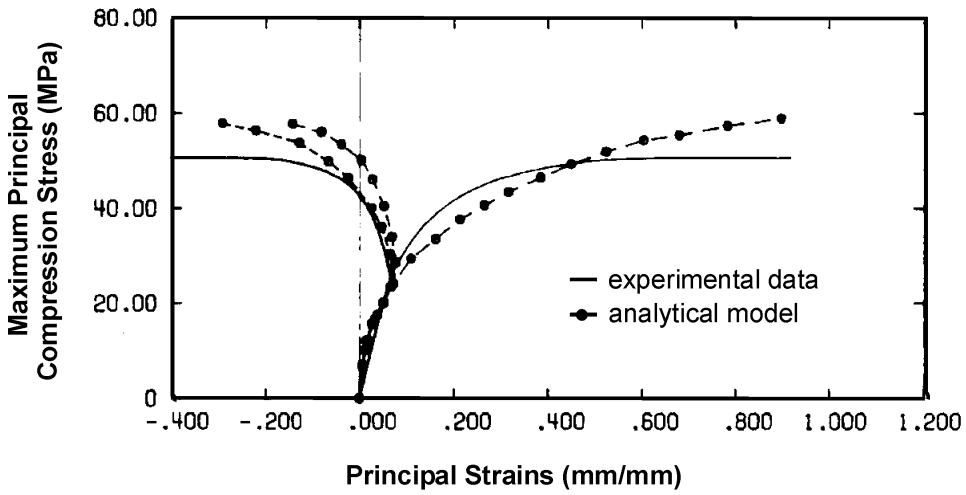

Figure 2.23:Predicted and Observed Concrete Response under Triaxial Compression (as Presented by Ohtani and Chen [1988])

with shear distortion of the material (Figure 2.13). For typical yield functions, this characteristic is contrary to the assumption of associated flow. Additionally, data show that concrete subjected to compressive loading exhibits nonlinear volume change, displaying contraction at low load levels and dilation at higher load levels (Figure 2.15). These characteristics of concrete response may be difficult to represent following the assumption of associated flow. In order to improve modeling of concrete material response some propose non-associated flow models in which the yield and plastic potential functions are not identical. Such models include that of Han and Chen, 1985; de Boer and Drenkamp, 1988; and Vermeer and de Borst, 1984.

The model proposed by Han and Chen [1985] follows from the assumption of non-associated flow in which the plastic potential function is defined to capture the variation in volumetric expansion as follows:

$$g(\sigma, q) = \alpha(k) I_1 + \sqrt{J_2} \tag{2-22}$$

where

$$\alpha(k) = \alpha_1 + \frac{\alpha_1 - \alpha_2}{k_y - k_f}(k - k_y) \tag{2-23}$$

and α_1, α_2 are material parameters, k maps between the initial yield surface (k_y) and the yield surface at maximum load (k_f). Figure 2.242.24 shows the computed stress-strain response for concrete subjected to biaxial loading compared with experimental data.

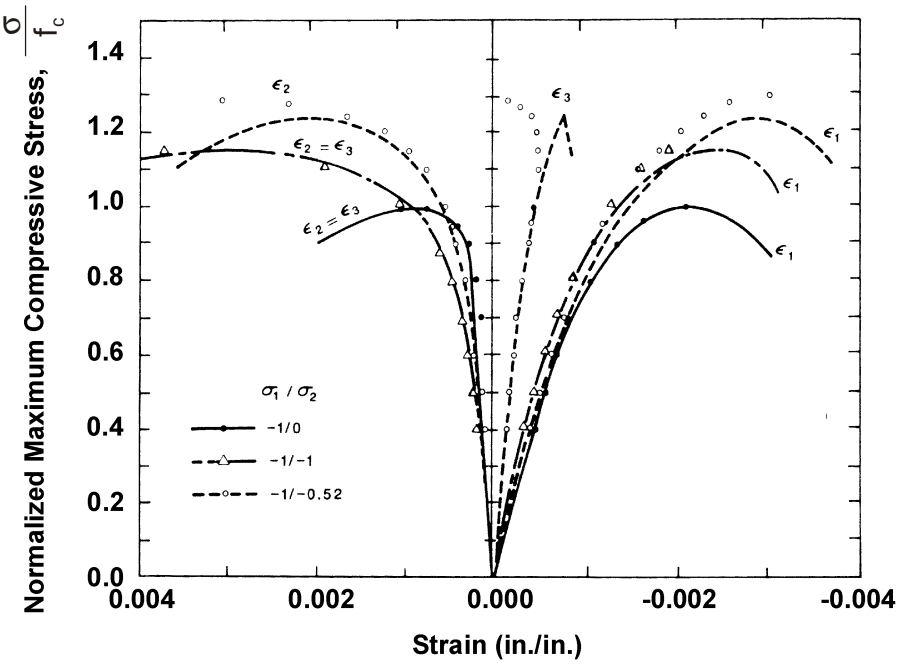

Figure 2.24:Predicted and Observed Stress-Strain Response for Concrete Subjected to Biaxial Loading (Data from Kupfer *et al.* [1969])

2.3.3 Damage Theory Applied to Modeling Concrete Behavior

The defining characteristic of material damage is reduced material stiffness. Experimental data exhibit material damage for concrete subjected to tensile loading, and to a lesser extent, compressive loading (see Figures 2.2 and 2.8). Thus, it is appropriate to incorporate material damage into models characterizing the response of plain concrete to variable loading. Continuum damage mechanics provides a means of modeling at the macroscopic level the material damage that occurs at the microscopic level. Development of a damage-based model requires definition of a damage rule that characterizes the rate at which material damage is accumulated and the orientation of the damage. Definition of this damage rule may also include definition of a damage surface that defines an initial

elastic domain. Various proposed damage models differ in the definition of the damage surface and damage rules.

Some of the first constitutive relationships for damaging materials proposed isotropic damage rules. One such model is that proposed by Lemaitre [1986]. This model follows from the assumption that one can define an effective stress that is larger than the Cauchy stress and accounts for the reduction in material area that results from microcracking:

$$\tilde{\sigma} = \frac{\sigma}{1 - D} \tag{2-24}$$

where $\tilde{\sigma}$ is the effective stress and D is the positive scalar measure of material damage. A second assumption follows that the material strain is a function of the effective stress. The contribution of damage to the thermodynamic potential for free energy in the system is explicitly defined:

$$\psi = \frac{1 - D}{2}\mathbf{C}:\mathrm{e}:\mathrm{e} \tag{2-25}$$

from which it follows ($\sigma = \partial_{\varepsilon}\psi$):

$$\tilde{\sigma} = (1 - D)\mathbf{C}:\tilde{\varepsilon} \tag{2-26}$$

and from which can be defined an internal variable associated with the damage state. Ultimately, a damage rule is proposed in which the rate of accumulated damage, $\dot{D}$ is a power function of the stress state. Chaboche [1988] proposes a very similar model in which the rate of accumulated damage is an explicit function of the strain state. These models can be calibrated to characterize the response of concrete subjected to uniaxial, cyclic loading However, these models imply that severe loading along one axis results in reduced material resistance to loading in any direction. Data collected during testing of reinforced concrete components indicate that this is not the most appropriate model for concrete subjected to multi-dimensional cyclic loading. Additionally, these models imply that dam-

age is accumulated immediately upon loading, an assumption that is not supported by material testing (Figure 2.8).

More recently anisotropic damage models have also been proposed. These models suggest that the orientation of damage is a function of the load history. One such model is that proposed by Resende and Martin [1984] in which different damage rules are proposed to characterize damage in the deviatoric and volumetric modes of response. Such a model is attractive given the clear effect of hydrostatic pressure on concrete response. However, calibration of such a model on the basis of standard material tests may be difficult. Additionally, as with the previously discussed isotropic models, it is not clear that severe loading in one direction necessarily reduces material capacity in other directions.

A second class of anisotropic models is proposed in which the orientation of material damage is a function of direction of loading. In the model proposed by Govindjee *et al.* [1995], a failure surface characterizes the initial elastic domain. A trial stress state, analogous to the trial stress state proposed for plasticity formulations, outside of the elastic domain indicates the initiation of material damage. As with the previously discussed isotropic damage models, the authors propose that the thermodynamic potential for the free energy of the system appropriately includes energy associated with material damage:

$$\Psi = \frac{1}{2}\mathbf{e}:\mathbf{D}:\mathbf{e} + S(\alpha) \tag{2-27}$$

However, here the free energy associated with accumulated damage, $S(\alpha)$, is not defined *a priori*; instead, the hypothesis of maximum dissipation is relaxed for softening materials from finding the minimum of the dissipation to finding the critical point. For appropriately defined damage surfaces, this results in damage flow rules that define the rate of change of the material compliance, **D**, and the internal damage variables, α, as follows:

$$\dot{\mathbf{D}} = \sum_{k=1}^{M} \gamma_k \frac{\partial_s \phi_k \otimes \partial_s \phi_k}{\partial_s \phi_k : \sigma} \tag{2-28a}$$

$$\dot{\alpha} = \sum_{k=1}^{M} \gamma_k (\partial_q \phi_k) \tag{2-28b}$$

where ϕ_k define the failure surfaces, γ_k are proportionality constants for loading of the surfaces and $A \otimes B$ represents the outer cross-product or tensors *A* and *B*. Thus, the orientation of damage is associated with orientation of the failure surfaces. These failure surfaces may be defined on the basis of the stress state at which damage initiates; analogous to the formation of a crack surface perpendicular to the direction of the maximum principal tensile stress. The authors propose an exponential softening rule for the failure surfaces and suggest that this softening rule can be calibrated on the basis of concrete fracture toughness.

The assumption of oriented damage incorporated in this model is conceptually pleasing. However, the authors proposed that the failure surfaces constrain the tensile and shear stresses transferred across a single fictitious crack surface, thereby allowing for unlimited strength and stiffness in directions parallel to the crack surface.

To address this issue, several models have been proposed in which the orientation of the active crack surfaces is allowed to change. One such method is to introduce multiple fixed fictitious crack surfaces [Litton, 1974; de Borst and Nauta, 1985; and Riggs and Powell, 1986]. For the model proposed by de Borst and Nauta, new fictitious fixed crack surfaces are introduced when the orientation of the principal stresses deviates from the orientation of the active cracks by a specified angle and stresses exceed a specified strength. Another approach is to allow the fictitious crack surface to rotate. Rots and Blaauwendraad [1989] suggest that the rotating crack model was first introduced by Cope et al. [1980] and later refined by others including Bazant [1983], Willam et al. [1987], Gupta

and Akbar [1984] and Crisfield and Wills [1989]. In rotating crack models, coaxality of the principal stresses and strains is assumed for each load increment. This assumption is enforced through variation of the material shear moduli. Rots and Blaauwendraad [1989] suggest that these two approaches are essentially the same provided that several conditions are satisfied.

- Formation of new crack surfaces depends solely on the orientation of the principal stress and not on the maximum stress state.
- Existing cracks are inactive upon formation of new crack surfaces
- The traction-strain law for the current crack accounts for previous cracks and enforces general coaxality of principal stresses and strains.

Of the variable crack models, the approach proposed by de Borst and Nauta [1985] is the most appropriate for modeling the response of reinforced concrete structural elements. This model provides a framework for introducing a few fictitious crack surfaces, the orientation of which is remembered and the activation of which depends on the stress state. Laboratory testing of reinforced concrete elements shows that discrete cracks form when principal stresses exceed concrete strength. As loading continues, these cracks may open or close depending on the load history. However, once formed, the concrete maintains a weakness in the direction of these cracks. Under load reversal additional cracks may form; however, typically the orientation of new cracks varies from the orientation of the initial cracks.

2.3.4 Elastic-Plastic-Damage Models for Concrete Response

Given that concrete displays the characteristics of both a plastic material and a damaging material, it is appropriate to develop models that incorporate both mechanisms of response. In recent years, two types of elastic-plastic-damage models have been proposed. Several of these models are developed on the basis of plasticity theory and the assumption that material damage appropriately is defined by the accumulated plastic strain [*e.g.*,

Frantziskonis and Desai, 1987; Lubliner *et al*., 1989]. The model proposed by Lubliner *et al.* [1989] has the following characteristics:

- The shape of the yield surface is assumed to remain constant and is defined by a modified Mohr-Coulomb criterion.
- The evolution of the elastic domain is defined by a hardening rule that is calibrated on the basis of experimental data.
- Plastic strain is defined on the basis of an associated flow rule.
- Damage is assumed to be isotropic and defined by a single scalar damage variable, κ, that is a measure of the accumulated damage.
- Damage is assumed to accumulated as a function of plastic strain:

$$\dot{\kappa} = \frac{r(\sigma)}{g_t} f_t(\kappa)\dot{\varepsilon}_1^p + \frac{1-r(\sigma)}{g_c} f_c(\kappa)\dot{\varepsilon}_3^p \tag{2-29}$$

  where ε_1^p and ε_3^p are the principal tensile and compressive strains; $f_t(\kappa)$ and $f_c(\kappa)$ are the hardening functions for concrete response in tension and compression; g_t is the concrete fracture toughness; g_c is a material parameter analogous to g_t but defined for compression response, and $r(\kappa)$ is a weighting function that characterizes the response as tensile or compressive in nature.

This models follows from the assumption that damage accumulated as a result of post-peak tensile loading will reduce concrete stiffness in compression; however, experimental testing of reinforced concrete elements under reversed cyclic loading indicates that this is not an appropriate assumption. This issue has been addressed by Lee and Fenves [1994] through the introduction of multiple damage parameters that defined concrete damage under predominantly compressive loading and predominantly tensile loading independently.

For a second class of elastic-plastic-damage elements, the damage and plasticity mechanism of response are independent. For these models, it is appropriate to consider the elastic domain to be bounded by the damage surfaces and the plasticity surfaces. One such

model is that proposed by Govindjee and Hall [1997]. This model considers a damage model to characterize the response of concrete in tension and shear and a plastic model to characterize the response of concrete in compression. Additionally, this model has the following characteristics:

- Anisotropic damage model with the orientation of damage established by formation of a single fixed fictitious crack surface that is perpendicular to the direction of the peak principal tensile stress.
- The damage/failure surface defines an undamaged concrete tensile strength and shear strength; damage initiates when the trial principal tensile strength exceeds the concrete tensile strength.
- The damage surface has an exponential softening rule with accumulated damage occurring through tensile and shear action on the fictitious crack surface.
- Single surface plasticity model with associated plastic flow.

This model has the advantages of the anisotropic, *crack-oriented* damage models previously identified. Additionally, the partial decoupling of the damage and plasticity modes of response provides enhanced numerical efficiency by allowing for consideration of only a single mode of response for appropriate trial stress states. It is possible for both the plasticity and damages surfaces to be active for a particular strain increment; thus, Govindjee and Hall [1997] propose a computationally efficient algorithm for solution of the stress state in this condition.

2.3.4.1 Objective Modeling of Concrete Behavior

Concrete subjected to severe compressive or tensile loading exhibits strain-softening characterized by reduced strength with increased deformation demand. For concrete loaded in tension, this response results from Mode I fracture. Thus, it appropriately is characterized by the concrete fracture energy as defined by the RILEM standard test procedure [RILEM, 1985] that measures the energy dissipated by a plane concrete beam sub-

jected to Mode I fracture. Using the finite element method and modeling concrete as a continuum requires distributing the damage associated with discrete cracking over a volume of material. The inconstancy between the concrete fracture energy that defines energy dissipation per unit crack area and the finite element model that defines energy dissipated per unit volume can be addressed through introduction of an element characteristic length. The need for consideration of the element characteristic length is supported further by the observation that the results of analysis using models that do not introduce a measure of mesh size exhibit severe dependency on the mesh discretization. A number of researchers have proposed methods for computing appropriate characteristic length values. Bazant and Oh [1983] introduce a crack-band width that is a function of the element area and the direction of the crack advancement. Crisfield [1986] proposes that the characteristic length be defined by the Jacobian at the individual Gausse points. Oliver [1989] introduces a general method for computing an element characteristic length that is a function of element size and the elastic stress state. These models shows mesh-independent results; in particular the model proposed by Oliver shows mesh-independent results for variable mesh patterns and stress fields.

Concrete loaded in compression also exhibits strain-softening. Results of similar studies by van Mier [1986] and by Lee and Willam [1997] show that the area under the stress-strain history for concrete prisms subjected to uniaxial compressive loading decreases with increasing prism height. This implies that compression failure is a localized phenomenon similar to concrete fracture. For the case of concrete loaded in compression, failure typically results from the development of variable-angle shear planes over the specimen height. For shorter specimens, more fracture surfaces form thereby resulting in a total energy dissipation that is approximately equal for specimens of variable height [van Mier, 1986]. However, calibration of the material response considering multi-Mode frac-

ture is not obvious, nor is consideration of an appropriate element characteristic length. Lubliner *et al.* [1989] propose that the area under the post-peak concrete compression stress-strain history be considered a material property and that an appropriate characteristic length be chosen such that the analytical results coincide with experimental results. Lee and Willam [1997] propose a crack density, h_c, that maps the area of crack surface under compression failure into the continuum volume. This crack density, h_c, could also be considered to be an element characteristic length. Here this parameter is defined on the basis of experimental data to be a function of the continuum element geometry:

$$\begin{aligned} h_c &= \frac{1}{10.5} h_{element} && \text{for simultaneous Mode I and Mode II fracture} \\ \frac{1}{3.75} h_{element} < h_c &< \frac{1}{2.25} h_{element} && \text{for Mode I fracture} \end{aligned} \tag{2-30}$$

where $h_{element}$ is a measure of the element length in the direction of the principal compressive stress, Model I refers to a fracture surface developed under purely tensile loading and Mode II refers to a fracture surface developed under in-plane shear loading. The authors present data showing that the analytical models compare well with the experimental data.

2.4 Characterization of the Response of Plain Concrete in Reinforced Concrete Beam-Column Bridge Joints

The experimental data presented in the preceding sections define the response of concrete subjected to variable loading. The previously discussed constitutive models provide a foundation for development of a model that characterizes the response of plain concrete. This information can be combined to develop a model that characterizes the modes of response exhibited by plain concrete in reinforced concrete beam-column bridge joints.

2.4.1 Characteristics of Reinforced Concrete Bridge Response

Data presented in Section 2.3 define the response of concrete subjected to multi-axial loading. However, consideration of reinforced concrete bridges suggest that the response of the system may be investigated through two-dimensional modeling. As discussed in Section 1.2, for many bridge systems, earthquake excitation perpendicular to the bridge is resisted through frame action while excitation parallel to the bridge is resisted at the bridge abutments. Since loading of the beam-column connection results from frame action, this loading is predominantly in the plane of the bridge frame. For bridge frames with square column, this loading results in a predominantly two-dimensional stress state. However, under moderate to severe loading, concrete expansion may activate transverse reinforcement to provide confinement in the out-of-plane direction. Thus, for these systems, the response may be characterized by a generalized plane stress model for which the out-of-plane shear stresses are assumed to be zero while the normal stress is defined to be a fixed value. For circular bridge columns, the assumption of generalized plane-stress is less accurate since flexural and shear response results in development of a fully three-dimensional stress field in which out-of-plane shear stresses are not negligible. However, even for a bridge frame with circular columns, the generalized plane stress model provides information about the mechanisms of system response.

2.4.2 Characteristics of Concrete Response

Consideration of the response of reinforced concrete beam-column connections, other reinforced concrete structural elements and plain concrete suggests a number of characteristics of concrete response that are necessary to development of an objective model of a reinforced concrete beam-column connection.

Loading of a reinforced concrete beam-column connection results from the flexural response of the beam and column members that frame into the joint. In order to predict the

response of the joint region, it is necessary to characterize the response of frame elements subjected to flexure and shear. Thus, the constitutive model developed for this study must predict the experimentally defined response of concrete subjected to uniaxial tensile loading and the deterioration of concrete shear transfer across crack planes. Additionally, the model must account for the response of concrete under compressive loading, including the observed response under uniaxial compressive loading and the observed effect of moderate confining pressure on compressive strength. Further, the model must account for the recovery of elastic concrete stiffness upon the transition from tensile to compressive loading.

The response of the reinforced concrete beam-column bridge connection may be determined by the strength and stiffness of the concrete within the immediate vicinity of the joint. Loading of the joint may result in cracking of the joint concrete when concrete principal stresses exceed the concrete tensile strength. Reduced concrete tensile and shear strength and stiffness in the direction of these cracks will result in redistribution of loads in the vicinity of the joint and thereby activate inelastic mechanisms of response. Upon load reversal, existing cracks will close and new cracks will form. Under earthquake loading of a bridge frame, beam-column connections are loaded predominately in shear. Load reversal represents a reversal in the connection shear stress and a 90 degree rotation of the principal stress axes. Thus, upon load reversal new cracks typically form approximately orthogonal to the initial cracks. This requires that the proposed concrete model predict reduced concrete strength and stiffness along orthogonal planes and predict recovery of concrete compression strength upon crack closure.

Experimental investigation of the response of reinforced concrete beam-column connections indicates that ultimate capacity of the system may depend on concrete compression response. As previously discussed, severe loading of a beam-column connection may

result in the deterioration of bond within the joint and the transfer of loads through a single concrete compression strut. Under these conditions, the ultimate capacity of the system depends on the response of the core concrete under compressive loading. Under compressive loading approaching capacity, the concrete will expand with the result that the transverse steel in the joint acts to confine the concrete. The rate at which the concrete loses compressive strength following loading to peak strength will be determined by the amount of confining pressure developed in the reinforcing steel. Because a goal of this study is to consider the rate at which connection load carrying capacity is lost, it is necessary to predict the volumetric expansion exhibited by the concrete.

Ultimate strength and post-peak response of a reinforced concrete beam-column joint may be determined by loss of concrete load capacity in tensile-type loading or in compression-type loading. The goal of this investigation is to identify the mechanisms associated with achieving ultimate capacity and to characterize the post-peak response of the system. Thus it is necessary that the constitutive model predict deterioration of material strength and stiffness in the vicinity of peak capacity for concrete subjected to variable loading.

2.4.2.1 Rate Dependence

Experimental data show that concrete strength and stiffness increase with the rate of loading. For plain concrete in reinforced concrete bridges subjected to earthquake loading, maximum strain rates are estimated to be 0.2 percent per second for tensile loading and 5 percent per second for compressive loading. At these strain rates, concrete tensile strength increases minimally, compressive strength increases less than 5 percent and elastic modulus increases by approximately 25 percent over that observed under pseudo-static loading conditions. These increases in strength and stiffness likely do not affect significantly structural response. Further, while the maximum concrete strain rates are estimates and may underestimate actual strain rates, additional factors support the assumption of

pseudo-static concrete material response introduced in the proposed material model. First, the increase in concrete strength with increasing strain rate is relatively shallow in the vicinity of the strain rates estimated to be associated with earthquake loading. An increase in the predicted concrete strain rate of 500 percent would introduce only a 10 percent increase in concrete tensile strength and a 10 percent increase in compressive strength. Second, for a bridge structure subjected to earthquake excitation, the period of time during which strain rates approach these peak values may be so limited that it is unnecessary to consider the effect of load rate. Also, the point in time at which load demand is maximum may not correspond to the point in time at which strain rate is maximum. Thus, damage may occur at moderate-to low load rates. Third, most experimental testing of reinforced concrete beam-column bridge joints subjected to simulated earthquake loading is completed using pseudo-static, displacement controlled loading. In order to verify the results of this analytical investigation through comparison with experimental data, it is necessary that material response be characterized under the pseudo-static load conditions. For these reasons, consideration of strain rate effects is considered an unnecessary complexity for this investigation.

2.4.3 Constitutive Theories Employed to Characterize Observed Concrete Response

Both plasticity and continuum damage theory are appropriately applied to represent the specific characteristics of concrete response identified in the preceding section. Consideration of experimental data and model characteristics indicates that a model developed on the basis of continuum damage theory is appropriate for representing the response of concrete subjected to severe tensile loading. Such a model predicts the reduction in strength and stiffness exhibited by plain concrete subject to tensile loading. Such a model does not predict unrecoverable deformation associated with severe tensile loading. However, this unrecoverable deformation is a minor fraction of the total deformation and thus

reasonably neglected. Here an anisotropic, fictitious-crack damage model is chosen as the most appropriate model for characterizing the directional deterioration of tensile strength and stiffness observed in reinforced concrete beam-column connections. Previously proposed models of this type employ one or several, fixed or rotating, fictitious crack surfaces. In the current implementation, two fixed orthogonal crack surfaces are considered the most appropriate model to represent the damage patterns observed in actual reinforced concrete structures. The orientation of the crack surfaces is determined under the elastic stress distribution.

Introduction of only two orthogonal crack surface does limit the generality of the proposed model; however, this limitation likely has little effect on the model's capacity to represent the response of most reinforced concrete bridge frames. Observation of laboratory models and structures damaged during recent earthquakes indicates that for most reinforced concrete frames subjected to earthquake loading, concrete cracking at a single point in the structure is limited to development of two approximately orthogonal cracks. Concrete response resulting from such cracking is represented well by the current model. It is reasonable to assume that for some structures activation of particular inelastic response mechanisms may result in reorientation of principal stress axes such that three or more concrete cracks develop at a single point in the structure. The proposed model does not directly represent these observed damage patterns. However, the deterioration of concrete strength and stiffness associated with development of more than two cracks is represented in part through increased action on the two orthogonal cracks included in the material model. This results in a predicted response that is slightly stiffer and stronger than is observed. However, since concrete fracture energy is minimal, this additional strength and stiffness associated with activation of the two orthogonal crack rather than a single, correctly oriented crack, likely has a limited impact on global response.

Calibration of the damage model requires consideration of material softening. Research indicates that system response is relatively insensitive to the shape of the softening branch of the tensile stress-deformation response [CEB, 1991]. Here an exponential curve is assumed to represent the response. However, research also indicates that the use of softening material models may result in mesh sensitivity that invalidates results. Concrete fracture energy is assumed to be a material parameter and is used to calibrate the softening branch of the tensile response. A damage material model characterizes energy dissipation as a function of the material volume; however laboratory testing suggests that energy is dissipated as a function of the generated crack surface area. Here an element characteristic length is introduced to ensure that the numerical energy dissipation is a function of material area rather than volume. Others have shown that the characteristic length method minimizes mesh sensitivity [Oh, 1983; Crisfield, 1986; Lee and Willam, 1997; Oliver, 1989]; similar results are observed in this study.

Consideration of material data and plasticity-model characteristics indicates that for the current investigation such a model is appropriate for representing the response of concrete subjected to compressive loading. A plasticity-type model predicts the accumulated deformation exhibited by concrete subjected to cyclic loading in compression. Also, such a model may be calibrated to represent strength deterioration associated with severe compressive strain demands. Plain concrete subjected to predominantly compressive loading in excess of that corresponding to the compressive strength does exhibit the deterioration of stiffness that is characteristic of material damage (Figure 2.5, Figure 2.4 and Figure 2.6). This behavior is not represented by a plasticity model, and such a model could be expected to over predict the unloading and reloading stiffness of crushed concrete. Research into the response of beam-column connections indicates that crushing of compression zones may control connection response [Paulay et al., 1978; Leon and Jirsa,

1986; Cheung et al., 1993; Pantazopoulou and Bonacci, 1994]. The goals of the current study are to predict the load distribution prior to failure, the failure mode of the system and the level of ductility associated with the final failure mode. These goals can be achieved by representing deteriorating compressive strength on the basis of a plasticity-type model. Representation of concrete material damage associated with severe compressive loading introduces additional computational effort and hampers objective calibration of the model. The additional complexity associated with introduction of a plastic-damage model does not warranty the improved representation of concrete behavior for a limited range of loading that does not directly support the project goals.

Typically a plasticity model is formulated on the basis of a yield surface defined in stress space. Material testing of concrete indicates that the Drucker-Prager yield criterion is a reasonable and simple representation of the yield surface for concrete subjected to biaxial compression and compression-tension type loading with zero to moderate levels of out-of -plane confinement. Data show that such a model may be calibrated on the basis of the out-of-plane confining pressure (see Figure 2.11). However, the range of loading for a reinforced concrete beam-column joint is relatively limited, thus it is reasonable to define a single yield surface that approximates response for the expected range of loading.

Definition of a plasticity type model requires characterization of the plastic flow. Here the assumption of associated plastic flow is used as a basis for characterizing the response. As previously discussed, the chosen yield surface and the assumption of associated flow has been shown to characterize the response of concrete subjected to compressive loading. Research conducted by others [e.g., Chen and Han, 1988] indicates that the assumption of associated flow may overestimate the plastic volumetric deformation observed in material testing and an appropriately calibrated non-associated flow model may yield more accurate prediction of concrete strains. However, the variability of experi-

mental data, the variable precision of all models in predicting concrete response under diverse load histories and enhanced numerical efficiency all support the use of an associated flow model.

Definition of a plasticity model also requires definition of the evolution of the plasticity yield surface. In this investigation it is assumed that the shape of the plasticity yield surface as defined by the Drucker-Prager yield criterion is maintained throughout the load history. Some researchers [e.g., Chen and Han, 1988] propose that under compression loading the yield surface appropriately evolves from a surface that defines a closed elastic region at the initial yield to a surface that characterizes unlimited strength under hydrostatic pressure at the maximum strength (see Section 2.2.7.2). However, since concrete in a reinforced concrete beam-column joint is subjected to only moderate pressure in the direction perpendicular to the frame, it is not necessary that the model accurately represent the response of concrete subjected to hydrostatic pressure. With the shape of the yield surface established, the hardening function id defined on the basis of the response of concrete in uniaxial compression. For the current implementation, an exponential function is calibrated on the basis of several typical concrete monotonic compression stress-strain data sets.

2.4.4 Definition of the Concrete Constitutive Model

The model developed to characterize the response of concrete for this investigation is an extension of the models previously proposed by Govindjee *et al.* [1995] and Govindjee and Hall [1997]. The formulation presented here provides for the formation of multiple fictitious crack surfaces, accounts for crack opening and closing, represents the response of concrete subjected to multi-dimensional loading in compression and predicts the response of concrete subjected to predominantly biaxial loading.

The model considers a body in three-dimensional space, $\Omega \in \Re^3$, composed entirely of the material considered here. Assuming that it is appropriate to model the material as a homogeneous continuum, each point in the body is assumed to obey the following relationship:

$$s = \mathbf{C}:(\varepsilon - \varepsilon^p) \tag{2-31}$$

where σ, ε, and ε^p are rank two stress tensors representing the Cauchy stress, the total strain and the plastic strain and $\mathbf{C}$ is the rank four tensor representing the material stiffness.

For this material, the elastic domain is bounded by a set of damage and plasticity surfaces. The three damage surfaces limit the normal and shear tractions across two, orthogonal, fictitious crack planes:

$$\Phi_1 = \mathbf{S}_1:\sigma - f_t + k_n q_{d_1} = 0 \tag{2-32a}$$

$$\Phi_2 = \mathbf{S}_2:\sigma - f_t + k_n q_{d_2} = 0 \tag{2-32b}$$

$$\Phi_3 = \left|\mathbf{S}_3:\sigma\right| - f_s + k_s\left(q_{d_1}\langle q_{d_1} - q_{d_2}\rangle^0 + q_{d_2}\langle q_{d_2} - q_{d_1}\rangle^0\right) = 0 \tag{2-32c}$$

where q_{d_1} and q_{d_2} are internal damage variables; k_n, k_s, f_t and f_s are material parameters, $\langle . \rangle^0$ is the McCauley bracket and the rank two tensors $\mathbf{S}_1$, $\mathbf{S}_2$ and $\mathbf{S}_3$ define the normal and shear tractions on two fictitious crack surfaces:

$$\mathbf{S}_1 = \mathbf{l} \otimes \mathbf{l} \tag{2-33a}$$

$$\mathbf{S}_2 = \mathbf{m} \otimes \mathbf{m} \tag{2-33b}$$

$$\mathbf{S}_3 = \frac{1}{2}(\mathbf{l} \otimes \mathbf{m} + \mathbf{m} \otimes \mathbf{l}) \tag{2-33c}$$

Note that the normals to the fictitious crack surfaces are defined by rank one tensors $\mathbf{l}$ and $\mathbf{m}$ with $\mathbf{l} \cdot \mathbf{m} = 0$. The boundary of the elastic domain is completed by a single plasticity yield surface, defined according to the Drucker-Prager yield criterion.

$$\Phi_4 = \|\mathbf{s}\| + \beta_p I_1 - q_p(\alpha_p) = 0 \tag{2-34}$$

where **s** is the deviatoric component of the stress tensor σ, I_1 is the first invariant of the stress tensor, α_p is an internal plasticity variable and q_p defines the evolution of the yield surface and all other constants are material parameters.

Assuming the material moduli to be variables, the free energy of the body is defined:

$$\Psi(\mathrm{e}^e, \mathbf{C}, \alpha_d, \alpha_p) = \frac{1}{2}\mathrm{e}^e : \mathbf{C} : \mathrm{e}^e + Sd(\alpha_d) + Sp(\alpha_p) \tag{2-35}$$

where e^e is the elastic strain tensor, α_d is a set of internal damage variables.

Govindjee *et al.* [1995] propose enforcement of the hypothesis of maximum dissipation as a means of deriving the damage flow rule. Here, assuming the damage and plasticity mechanisms to be uncoupled, this technique can be used to derive both the damage and plasticity flow rules. In the absence of thermal effects, the internal dissipation E is defined:

$$E = -\dot{\Psi} + \mathrm{s} : \dot{\mathrm{e}} \tag{2-36}$$

It follows from Equations (2-31) and (2-35) that

$$E = \frac{1}{2}\sigma : \dot{\mathbf{D}} : \mathrm{s} + \mathrm{s} : \dot{\mathrm{e}}^p + q_d \cdot \dot{\alpha}_d + q_p \dot{\alpha}_p \tag{2-37}$$

where $\dot{\mathrm{e}}^p$ is the plastic strain rate and $\dot{\mathbf{D}}$ is the rate of change of the material compliance tensor. Govindjee *et al.* [1985] suggest that the hypothesis of maximum dissipation cannot be strictly enforced in the case of materials that exhibit softening. Instead it is appropriate to consider the critical point. Here the associate Lagrangian is defined:

$$L(\sigma, q_d, q_p) = -E + \sum_{k=1}^{4} \gamma_k \Phi_k \tag{2-38}$$

where γ_k are generalized Lagrange multipliers. The critical point of this Lagrangian is defined by

$$\partial_\sigma \mathrm{L} = 0 \tag{2-39a}$$

$$\partial_{q_p} \mathrm{L} = 0 \text{ and } \partial_{q_d} \mathrm{L} = 0 \tag{2-39b}$$

$$\Phi_k \le 0 \qquad \gamma_k \ge 0 \qquad \gamma_k \Phi_k = 0 \tag{2-39c}$$

Here it is assumed that the Lagrangian multipliers that define the critical point of the dissipation may be determined through an incremental solution algorithm in which the damage and plasticity mechanisms are uncoupled [Govindjee and Hall, 1997]. This requires solving the optimization problem assuming no increase in damage or no increase in plastic deformation. The equations defining the optimization problem for the decoupled damage and plasticity mechanisms are as follows:

$$\dot{\mathbf{D}} = \sum_{k=1}^{3} \gamma_k \frac{\partial_\sigma \Phi_k \otimes \partial_\sigma \Phi_k}{\partial_\sigma \Phi_k : \sigma} \tag{2-40a}$$

$$\dot{\alpha}_d = \sum_{k=1}^{3} \gamma_k (\partial_{q_d} \Phi_k) \tag{2-40b}$$

$$\dot{e}^p = \gamma_4 (\partial_s \Phi_4) \tag{2-40c}$$

$$\dot{\alpha}_p = \gamma_4 (\partial_{q_p} \Phi_4) \tag{2-40d}$$

These flow rules are constrained by the consistency condition and the Kuhn-Tucker conditions (defined as the constraints of optimization in Equation (2-39c)):

$$\gamma_k \dot{\Phi}_k = 0 \tag{2-41a}$$

$$\Phi_k \le 0 \qquad \gamma_k \ge 0 \qquad \gamma_k \Phi_k = 0 \tag{2-41b}$$

Definition of the constitutive relationship requires establishment of criteria governing crack opening and closure. Here it is assumed that if the stress normal to the orientation of a fictitious crack plane is tensile, then the crack is open and deterioration of material stiffness associated with the particular crack is realized. However, if the stress is compressive, the crack is considered to be closed and elastic material properties are recovered. These assumptions are formalized as follows:

$$\boldsymbol{D}^n = \begin{cases} \boldsymbol{D}_{elastic} & \boldsymbol{S}_1 : \sigma^{n+1} \le 0 \quad and \quad \boldsymbol{S}_2 : \sigma^{n+1} \le 0 \\ \boldsymbol{D}^n_{\alpha_{d_1}} & \boldsymbol{S}_1 : \sigma^{n+1} > 0 \quad and \quad \boldsymbol{S}_2 : \sigma^{n+1} \le 0 \\ \boldsymbol{D}^n_{\alpha_{d_2}} & \boldsymbol{S}_1 : \sigma^{n+1} \le 0 \quad and \quad \boldsymbol{S}_2 : \sigma^{n+1} > 0 \\ \boldsymbol{D}^n_{\alpha_d} & \boldsymbol{S}_1 : \sigma^{n+1} > 0 \quad and \quad \boldsymbol{S}_2 : \sigma^{n+1} > 0 \end{cases} \tag{2-42}$$

where $\boldsymbol{D}_{elastic}$ is the elastic material compliance, $\boldsymbol{D}^n_{\alpha_{d_k}}$ is the material compliance accounting for accumulated damage in the direction of fictitious crack surface k and $\boldsymbol{D}^n_{\alpha_d}$ is the material compliance accounting for accumulated damage in the direction of both fictitious crack surfaces.

Definition of the constitutive model is completed by a series of three *generalized* hardening rules that characterize the evolution of the damage and plasticity surfaces as a function of the accumulated damage and plastic strain. As previously discussed, here it is assumed that the deterioration of concrete tensile strength is reasonably approximated as exponential. Thus the damage variables q_d are defined as follows:

$$q_{d_k}(\alpha_{d_k}) = f_t(1 - \exp(-H\alpha_{d_k})) \tag{2-43}$$

where the hardening parameter H is assumed to be a function of the concrete fracture energy. The plasticity hardening function characterizes the evolution of the yield surface. Here a six-parameter function is used to characterize the observed response of concrete subjected to uniaxial compression loading:

$$q_p(\alpha_p) = Y_0(A\exp(a\alpha_p) + B\exp(b\alpha_p) + C\exp(c\alpha_p)) \tag{2-44}$$

where the hardening parameters a, b, and c are assumed to be a function of the concrete energy dissipation in compression.

2.4.4.1 Energy Dissipation under Strain-Softening and the Element Characteristic Length

For materials such as concrete that exhibit strain softening, it is necessary to consider the energy dissipation associated with activation of the softening mechanism in calibration of the material constitutive model. For the model developed for use in this investigation, material softening is assumed to result from localized damage. For the case of concrete loaded in tension, this localized damage is the formation and propagation of discrete cracks perpendicular to the orientation of the principal tensile stress. For concrete loaded in compression, the damage pattern proposed by van Mier [1986] is considered to be an appropriate model. Here compressive deformation is assumed to result from the formation of multiple shear-type cracks the density of which is a function of the length of the specimen parallel to the direction of the principal compressive stress.

Both of these models for concrete damage imply that an appropriate element characteristic length is a measure of the element parallel to the direction of the principal tensile and compressive stress. As defined in Equation (2-36) energy dissipation per unit volume is as follows:

$$E = -\dot{\Psi} + \mathbf{s}:\dot{\boldsymbol{\varepsilon}} \tag{2-45}$$

For concrete loaded in uniaxial tension, the proposed model as define by Equations (2-35), (2-40a), (2-43) and (2-45) implies that the total energy dissipated through Mode I fracture, g_t, is as follows:

$$g_t = \int\left(\frac{1}{2}\dot{\varepsilon}\sigma - \frac{1}{2}\dot{\sigma}\varepsilon + f_t\left(\dot{\varepsilon} - \frac{\varepsilon}{\sigma}\dot{\sigma}\right)\right) \tag{2-46}$$

where the total dissipation is defined over the history from zero to complete damage. Expressions for the strain rate and stress rate appropriately are determined from an experimental data. This experimentally determined energy dissipation is defined as energy per

unit volume of material. Introduction of the experimental gage length results in a definition of concrete fracture energy per unit area of crack surface as follows:

$$G_t = \int \frac{1}{2}\sigma\dot{u} - \frac{1}{2}\dot{\sigma}u + f_t \cdot \left(\dot{u} - \frac{u}{\sigma}\dot{\sigma}\right) \tag{2-47}$$

where $u = \varepsilon \cdot l_{gage}$. It is important to note that the model-consistent concrete fracture energy as defined by Equation (2-47) is not precisely the same value as that defined by the standard concrete fracture energy test [RILEM, 1985]:

$$G_t = \int \sigma\dot{u} \tag{2-48}$$

For this investigation, the consistent concrete fracture energy is used for cases in which the experimental test data is available and the fracture energy as defined by the standard procedures is used for all other cases.

With the concrete fracture energy defined by experimental data, the tension softening regime of the current model is calibrated on the basis of the following equations:

$$g_t = \int \frac{1}{2k_n}\dot{\alpha}_d(f_t - k_n q_d) + q_d\dot{\alpha}_d \tag{2-49}$$

assuming a limit point defining *substantial material damage*, the model parameters is defined

$$H = l\frac{f_t}{2G_t}\left(\lambda\left(1 + \frac{1}{k_n}\right) - (1 - \exp(\lambda))\right) \tag{2-50}$$

where $\lambda = H\alpha_d$ corresponds to a value of α_d for which q_d achieves a predefined limit value that defines *substantial material damage* and l is the element characteristic length. Here the definition of element characteristic length as proposed by Oliver [1989] and as implemented by Govindjee and Hall [1997] is used.

For concrete subjected to uniaxial loading in compression, the proposed model as defined by Equations (2-31), (2-37), (2-40a) and (2-45) implies that the total energy dissipated through damage in compression is as follows:

$$g_c = 2\int_{\Gamma} \sigma \dot{\varepsilon}_p d\Gamma = 2\int_{\Gamma} q \dot{\alpha}_p d\Gamma \tag{2-51}$$

where Γ defines the history from the point of maximum compressive strength through a limited residual compressive strength. Experimental data indicate that compression softening is associated with the development of localized failure mechanisms. Thus, the energy dissipation per material area associated with compression failure may be defined through Equation (2-51) with the plastic strain defined as a function of the experimental gage length:

$$G_c = l_{gage}\int_{\Gamma} 2\sigma\left(\dot{\varepsilon} - \frac{\varepsilon}{\sigma}\dot{\sigma}\right) d\Gamma \tag{2-52}$$

Lee and Willam [1997] suggest that the appropriate gage length is a function of the assumed mode of failure; however, the relationship between the true gage length and the analytical gage length would be the same for both computation of concrete plastic energy dissipation and for calibration of the material model. Following the process used for calibration of the constitutive model in tension, the model is calibrated for compression-type loading:

$$\int_{\Gamma} q \dot{\alpha}_p d\Gamma = \frac{G_c}{2l} \tag{2-53}$$

where l_c is the element characteristic length and defines a measure of the element parallel to the orientation of principal compression stress at the point at plastic deformation is initiated.

2.4.5 Implementation of the Model in an Implicit Incremental Solution Algorithm

Constitutive models such as the one presented here may be utilized to solve a variety of problems. Often such a model is implemented in a computer code that uses the finite element or finite difference method to solve a given boundary value problem. Typically,

these codes employ the following techniques. An implicit incremental solution algorithm is used to advanced the solution from a known state of the system at time t^n to a solution at time t^{n+1} given a load increment applied in the interval $\Delta t = t^{n+1} - t^n$. A displacement-based method is used in which the displacement field in the body, while not necessarily the correct displacement field, is considered a known quantity. At the level of the constitutive model, this algorithm requires the following, given a known *state* at time t^n and the strain at time t^{n+1}, the constitutive model is used to predict the *state* at time t^{n+1}. For the concrete constitutive model defined here, the material state is uniquely defined by seven internal variables. In addition to predicting the material state at time t^{n+1}, the global solution algorithm also requires calculation of a material tangent that defines the change in material stress as a function of material strain.

2.4.5.1 Integration of the Flow Rules

A variety of numerical integration methods have been suggested for advancement of the material solution state. Here, the Backward Euler method is used since this method provides unconditional stability and first order accuracy:

$$\begin{aligned} x^{n+1} &= x^n + \Delta t f(x^{n+1}) \\ f(x^{n+1}) &= \left.\frac{\partial x}{\partial t}\right|_{n+1} \end{aligned} \tag{2-54}$$

A solution at time t^n implies that the following system and internal variables are known: s^n, e_p^n, $\boldsymbol{D}^n$, $\alpha_{d_1}^n$, $\alpha_{d_2}^n$, α_p^n. Additionally, it is assumed that at time t^{n+1} the strain state ε^{n+1} is known. Given that the material constitutive parameters are a function of the level of system damage, the stress state at time t^n is an appropriate characteristic of the material state rather than the strain state. Integrating the flow rules defined by Equation (2-40a) through (2-40d) and using the damage and yield surfaces defined by Equations (2-32a) through (2-32c) and (2-34) results in the following system of equations:

$$\boldsymbol{D}^{n+1} = \boldsymbol{D}^{n} + \gamma_1 \frac{\boldsymbol{S}_1 \otimes \boldsymbol{S}_1}{\boldsymbol{S}_1 : \sigma^{n+1}} + \gamma_2 \frac{\boldsymbol{S}_2 \otimes \boldsymbol{S}_2}{\boldsymbol{S}_2 : \sigma^{n+1}} + \gamma_3 \frac{\boldsymbol{S}_3 \otimes \boldsymbol{S}_3}{\boldsymbol{S}_3 : \mathrm{s}^{n+1}} \tag{2-54a}$$

$$\alpha_{d_1}^{n+1} = \alpha_{d_1}^{n} + k_n \gamma_1 + k_s \gamma_3 \langle q_{d_1}^{n+1} - q_{d_2}^{n+1} \rangle^0 \tag{2-54b}$$

$$\alpha_{d_2}^{n+1} = \alpha_{d_2}^{n} + k_n \gamma_2 + k_s \gamma_3 \langle q_{d_2}^{n+1} - q_{d_1}^{n+1} \rangle^0 \tag{2-54c}$$

$$\alpha_p^{n+1} = \alpha_p^{n} + \gamma_4 \tag{2-54d}$$

$$\mathrm{e}_p^{n+1} = \varepsilon_p^{n} + \gamma_4 \frac{\partial \Phi_4}{\partial \mathrm{s}} \Bigg|^{n+1} \tag{2-54e}$$

where the definition of the Lagrange multipliers is updated to be $\gamma_k = \Delta t \gamma_k^{n+1}$. Combining the integrated flow rules (Equation (2-54)) with the material constitution defined in Equation (2-31) and the surface criteria defined in Equations (2-32a) through (2-32c) and (2-34), results in a system of seven, coupled, non-linear equations subject to the constraints of Equation (2-41a) and (2-41b) and Equation (2-42):

$$\sigma^{n+1} = \boldsymbol{C}^{n} : \left(\varepsilon^{n+1} - \varepsilon_p^{n} - \gamma_4 \frac{\partial \Phi_4}{\partial \sigma} \Bigg|^{n+1} \right) \tag{2-55a}$$

$$\Phi_1 = \boldsymbol{S}_1 : \sigma^{n+1} - f_t + k_n q_{d_1}^{n+1} = 0 \tag{2-55b}$$

$$\Phi_2 = \boldsymbol{S}_2 : \mathrm{s}^{n+1} - f_t + k_n q_{d_2}^{n+1} = 0 \tag{2-55c}$$

$$\Phi_3 = \left| \boldsymbol{S}_3 : \mathrm{s}^{n+1} \right| - f_s + k_s \left(q_{d_1} \langle q_{d_1} - q_{d_2} \rangle^0 + q_{d_2} \langle q_{d_2} - q_{d_1} \rangle^0 \right) \Bigg|^{n+1} = 0 \tag{2-55d}$$

$$\Phi_4 = \left\| \boldsymbol{s}^{n+1} \right\| + \beta_p I_1^{n+1} - q_p(\alpha_p^{n+1}) = 0 \tag{2-55e}$$

This provides sufficient constraint to solve for the seven internal variables that uniquely define the solution at time t^{n+1}: $\gamma_1, \gamma_2, \gamma_3, \gamma_4, \varepsilon_p^{n+1}$ (note that the plastic strain tensor, ε_p^{n+1}, comprises three unique plastic strains). The material state is defined by the seven coupled equations if there is plastic flow and accumulated damage on all of the fictitious crack surfaces; for most cases only one or two damage/plasticity surfaces are active and the number of equations defining the material state is reduced.

2.4.5.2 Algorithm for Solution of the Governing Equations

If all damage and yield surfaces are active, determination of the material state at time t^{n+1} may require solution of a reduced set of seven coupled, non-linear equations. However, it is most likely that the damage surfaces and the plasticity surface will not be simultaneously active. Thus, in order to enhance the efficiency of the solution algorithm for the most common material states, Govindjee and Hall [1997] suggest incremental enforcement of coupling between the plasticity and damage mechanisms. A quasi-Newton solution algorithm is proposed in which the system is solved for the three consistency parameters associated with the damage surfaces assuming no change in the plastic strain increment and then the system is solved for the four internal plasticity variables assuming no change in the damage level. The material state is continuously updated until there is no increase in material damage or plastic strain.

Since it is not possible to know which surfaces are active or which cracks are open a predictor-corrector algorithm is used for solution of the material state. This method, the classical return mapping algorithm, defines a predictive stress state (the trial stress) to be elastic as defined by $\gamma_k = 0$ and $e_p^{n+1} = e_p^n$. The material compliance as defined in Equation (2-54) also is taken to be a function of the trial stress state, defined by $\gamma_k = 0$, and is equal to the material compliance at the end of the previous time step. The trial stress state is used to determine which cracks are open and which surfaces are active. If the trial stress state satisfies the damage/yield surface criteria, then no surfaces are active and the trial stress is the true stress. If the trial stress state implies that particular surfaces are active, then the solution proceeds assuming that only those particular surfaces are active. Once a solution is found that satisfies the constraints of the surfaces assumed to be active, the solution is considered to be valid only if it satisfies all of the governing equations for

the system and the associated constraints. If a solution is found to be invalid, active surfaces are added and dropped as is appropriate to provide a new trial stress.

2.4.5.3 Solution Algorithm for Single Surface Plasticity

The case of single surface plasticity requires solution of a series of four coupled non-linear equations. Substitution of the integrated flow rules into the plasticity yield surface criteria, assuming an elastic trial stress state, result in the following system of equations:

$$\Phi_4 = \left\| \boldsymbol{s}^{n+1} \right\| + \beta_p I_1(\sigma^{n+1}) - q_p(\alpha_p^n, \gamma_4) = 0 \tag{2-56a}$$

$$\sigma^{n+1} = \sigma_{trial}^{n+1} - \gamma_4 \boldsymbol{C}^n : \frac{\partial}{\partial \sigma} \Phi_4(\sigma^{n+1}) \tag{2-56b}$$

where

$$\frac{\partial}{\partial \sigma} \Phi_4(\sigma) = \frac{s_{ij}}{\|\boldsymbol{s}\|} + \beta_p \delta_{ij} \tag{2-56c}$$

$$q_p(\alpha_p^n, \gamma_4) = Y_0 \left(\begin{array}{c} A \exp(a(\alpha_p^n + \gamma_4)) + B \exp(b(\alpha_p^n + \gamma_4)) \\ + C \exp(c(\alpha_p^n + \gamma_4)) \end{array} \right) \tag{2-56d}$$

With the Drucker-Prager yield criteria it is not possible to further simplify this system into a single equation with one unknown variable. Observation of the solution of this system shows that the coupling between the equations can be significant. As a result, the orientation of the plastic strain increment as predicted using the trial stress state can differ substantially from the orientation of the true stress and the radius of convergence of the classical Newton solution algorithm can be impractically small. Rather than improving the initial value used in the solution algorithm, a line search algorithm [Matthies and Strang, 1979] is implemented for cases in which the Newton solution algorithm fails to converge.

2.4.5.4 Solution Algorithm for Single- and Multi-Surface Damage

The case of single- or multi-surface damage requires solution of a system of one to three coupled, non-linear equations. Substitution of the integrated flow rules into the dam-

age surface criteria and assuming an elastic trial stress state, results in the following system of three non-linear, coupled equations that must be solved for the damage consistency parameters:

$$\Phi_1 = \boldsymbol{S}_1:\sigma_{trial}^{n+1} - \gamma_1 \boldsymbol{S}_1:\boldsymbol{C}^n:\boldsymbol{S}_1 - \gamma_2 \boldsymbol{S}_1:\boldsymbol{C}^n:\boldsymbol{S}_2 - f_t + k_n q_{d_1}\left(\alpha_{d_1}^n, \gamma_1, \gamma_3\right) = 0 \qquad (2\text{-}56a)$$

$$\Phi_2 = \boldsymbol{S}_2:\sigma_{trial}^{n+1} - \gamma_1 \boldsymbol{S}_2:\boldsymbol{C}^n:\boldsymbol{S}_1 - \gamma_2 \boldsymbol{S}_2:\boldsymbol{C}^n:\boldsymbol{S}_2 - f_t + k_n q_{d_2}\left(\alpha_{d_2}^n, \gamma_2, \gamma_3\right) = 0 \qquad (2\text{-}56b)$$

$$\Phi_3 = \left|\boldsymbol{S}_3:\sigma_{trial}^{n+1}\right| - \gamma_3 \boldsymbol{S}_3:\boldsymbol{C}^n:\boldsymbol{S}_3 - f_t + k_n q_{d_3}\left(\alpha_{d_1}^n, \alpha_{d_2}^n, \gamma_1, \gamma_2, \gamma_3\right) = 0 \qquad (2\text{-}56c)$$

where

$$\sigma_{trial}^{n+1} = \boldsymbol{C}^n:(\varepsilon^{n+1} - \varepsilon_p^n) \qquad (2\text{-}56d)$$

$$\gamma_k \geq 0 \qquad (2\text{-}56e)$$

The above system of equations utilizes the stiffness orthogonality of the crack surfaces identified by Govindjee *et al.* [1985]: $\boldsymbol{S}_1:\boldsymbol{C}:\boldsymbol{S}_3 = \boldsymbol{S}_2:\boldsymbol{C}:\boldsymbol{S}_3 = 0$. For the special case of only one crack open, the stiffness orthogonality of the system may be exploited in updating the material stiffness. In this case the Sherman-Morrison-Woodbury formula [Golub, 1989] may be used to develop a simplified method for directly updating the material stiffness:

if

$$\boldsymbol{D}_{\alpha_{d_k}}^{n+1} = \boldsymbol{D}_{\alpha_{d_k}}^{n} + \gamma_k \frac{\boldsymbol{S}_k \otimes \boldsymbol{S}_k}{\boldsymbol{S}_k:\sigma^{n+1}} + \gamma_3 \frac{\boldsymbol{S}_3 \otimes \boldsymbol{S}_3}{\boldsymbol{S}_3:\sigma^{n+1}} \qquad (2\text{-}57a)$$

then

$$\boldsymbol{C}_{\alpha_{d_k}}^{n+1} = \boldsymbol{C}_{\alpha_{d_k}}^{n} - \left(\frac{\boldsymbol{C}_{\alpha_{d_k}}^{n}:\boldsymbol{S}_k \otimes \boldsymbol{C}_{\alpha_{d_k}}^{n}:\boldsymbol{S}_k}{\frac{1}{\gamma_k}\boldsymbol{S}_k:\sigma^{n+1} + \boldsymbol{S}_k:\boldsymbol{C}_{\alpha_{d_k}}^{n}:\boldsymbol{S}_k} + \frac{\boldsymbol{C}_{\alpha_{d_k}}^{n}:\boldsymbol{S}_3 \otimes \boldsymbol{C}_{\alpha_{d_k}}^{n}:\boldsymbol{S}_3}{\frac{1}{\gamma_3}\boldsymbol{S}_3:\sigma^{n+1} + \boldsymbol{S}_3:\boldsymbol{C}_{\alpha_{d_k}}^{n}:\boldsymbol{S}_3} \right) \qquad (2\text{-}57b)$$

where *k = 1,2.*

2.5 Comparison of Material Model with Experimental Data

The proposed concrete constitutive model is implemented in the finite element program FEAP [Taylor, 1998; Zienkiwiez and Taylor, 1987 and 1991]. This implementation is used to analyze the response of plain concrete systems subjected to various load histories. The behavior of plain concrete as predicted by the material model is compared with experimentally observed response for a variety of load histories including uniaxial, cyclic compression; uniaxial, cyclic tension, uniaxial reversed cyclic loading; and multi-dimensional loading. Additionally, the objectivity of the model is investigated for loading in compression and tension.

Figure 2.25 shows the predicted and experimentally observed response of concrete subjected to uniaxial, monotonic compression loading. Given the wide variation in experimental data, calibration of the model to represent the results of a single experimental test is inappropriate. Instead, the model is calibrated to predict the typical response of concrete. .

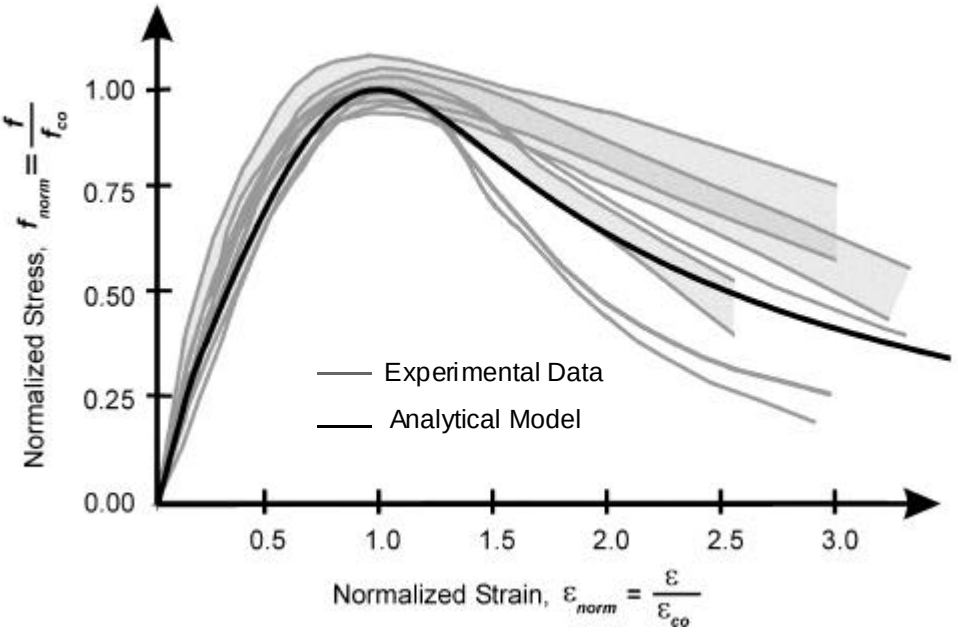

Figure 2.25:Predicted and Observed Compressive Stress-Strain Response for Concrete (Experimental Data as Presented in Figure 2.5)

Figures 2.26 and 2.27 show good correlation between predicted and experimentally observed response for concrete subjected to uniaxial, cyclic compression loading. In general, the model represents well the fundamental characteristics of concrete response. One exception is that for maximum concrete strains in excess of that corresponding to maximum compressive strength, the model does not predict the observed reduction of elastic material modulus and over-estimates the accumulation of plastic strain. These differences between the predicted and observed response follow from the assumption of a plasticity-based analytical model. However, given that the goal of this investigation is to predict the mechanisms of load transfer associated with achieving maximum strength of a reinforced concrete bridge joint, differences between the predicted and observed response are not expected to greatly affect the results.

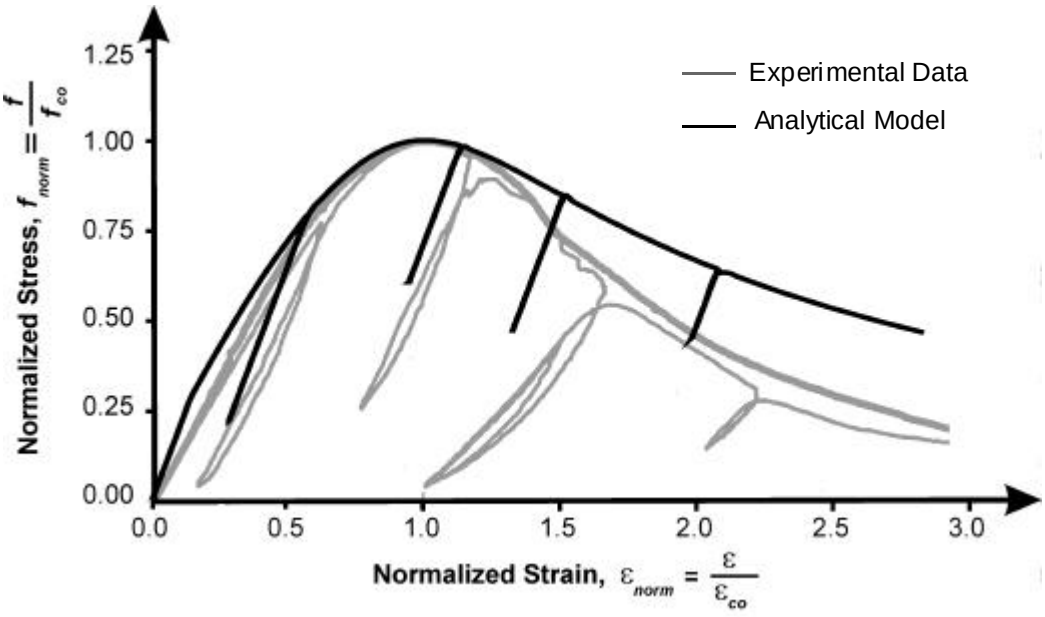

Figure 2.26:Predicted and Observed Stress-Strain Response for Concrete Subjected to Uniaxial, Cyclic Compression Loading (Data as presented in Figure 2.2)

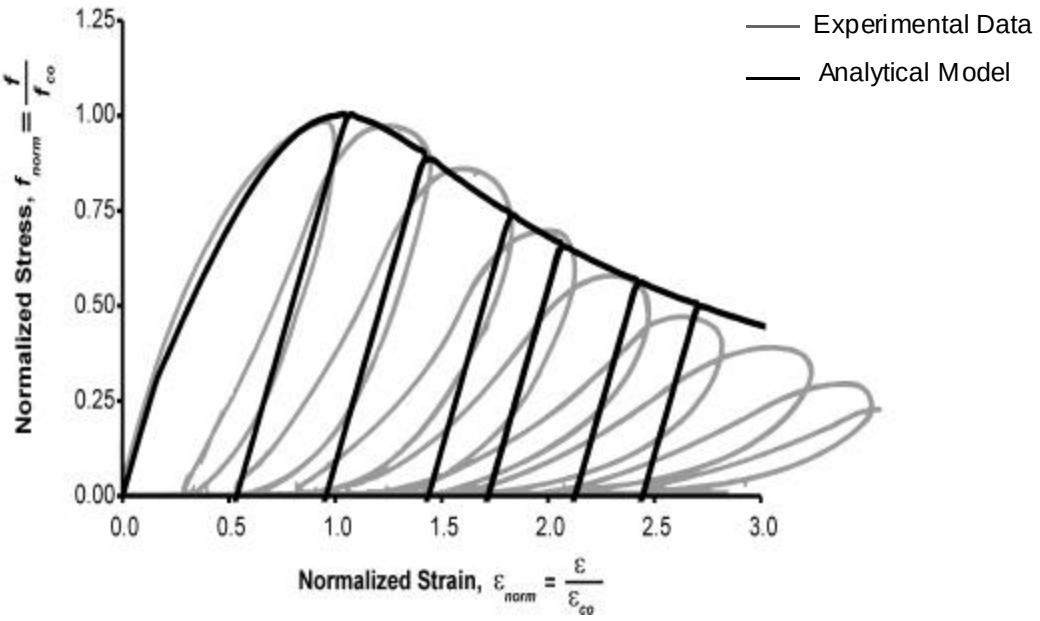

Figure 2.27:Predicted and Observed Normalized Stress-Strain Response for Concrete Subjected to Uniaxial, Cyclic Compression Loading (Experimental Data as Presented in Figure 2.4)

The response of concrete subjected to uniaxial monotonic and cyclic tensile loading is presented in Figures 2.28, 2.29 and 2.30. These data show that the analytical model characterizes the fundamental aspects of the concrete response. Results obtained from analytical modeling use the definition of concrete fracture energy associated with the model rather than the definition defined by the RILEM standard [1985]. Figure 2.28 shows observed and predicted stress-strain response for concrete subjected to uniaxial tensile loading. Here all observations and the analysis distribute the damage over the same specific gage length; thus it is appropriate to consider the average tensile strain over the gage length. Data presented in Figure 2.28 show that the models represents the typical response of concrete subjected to monotonic loading. Figure 2.29 presents data for concrete subjected to cyclic tensile loading, these data show that the analytical model predicts a greater reduction in elastic modulus than is observed. However, data presented in Figure

2.30 show that the reduced material stiffness does predict the response of concrete subjected to reversed cyclic loading with acceptable accuracy.

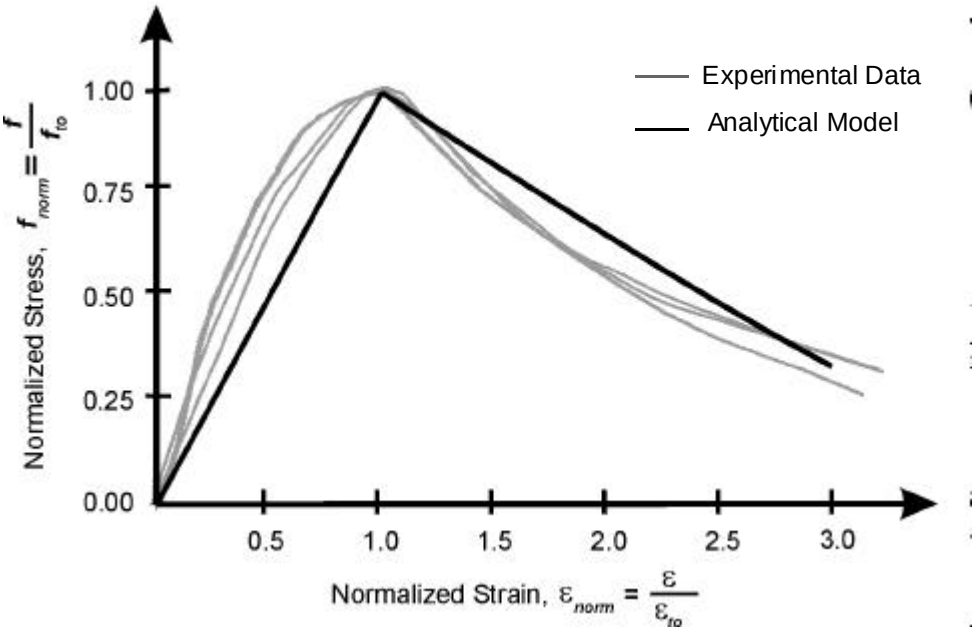

Figure 2.28:Predicted and Observed Normalized Concrete Tensile Stress-Strain Histories (Experimental Data as Presented in Figure 2.7)

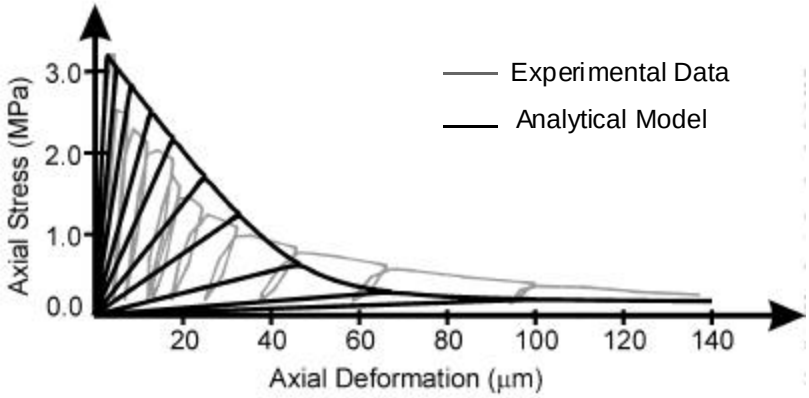

Figure 2.29:Typical Response of Concrete Subjected to Uniaxial, Cyclic Tensile Loading (Experimental Data as Presented in Figure 2.8)

The response of concrete subjected to biaxial and generalized plane stress loading are presented in Figure 2.31. Figure 2.31 shows the relationship between maximum normalized deviatoric stress and the maximum first invariant of the stress state. The model characterizes the average response for concrete subjected to compressive-type loading in the

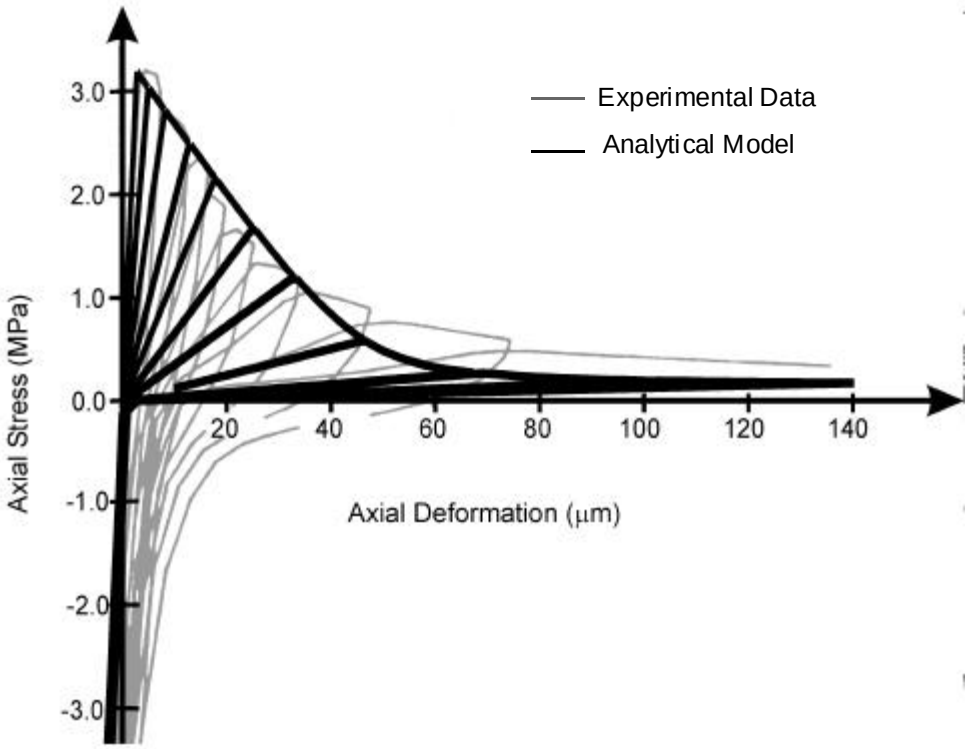

Figure 2.30:Typical Response of Concrete Subjected to Reversed Cyclic Loading with Failure in Tension (Data as Presented in Figure 2.9)

range of nominal pressure that concrete in reinforced concrete bridge beam-column joint may be expected to experience.

Figure 2.32 presents the relationship between volumetric strain and maximum normalized compressive stress. As previously discussed, representation of the volumetric expansion is important for predicting the response of reinforced concrete beam-column connections, since volumetric expansion activates steel reinforcement and may determine the mechanism of response. The analytical model predicts the fundamental characteristics of the response. The analytical model is calibrated to predict the typical response of concrete subjected to biaxial and general plane stress loading (see Figure 2.31). This calibration over-estimates the strength of concrete subjected to biaxial loading as observed by Kupfer [1969], as is shown in Figure 2.32.

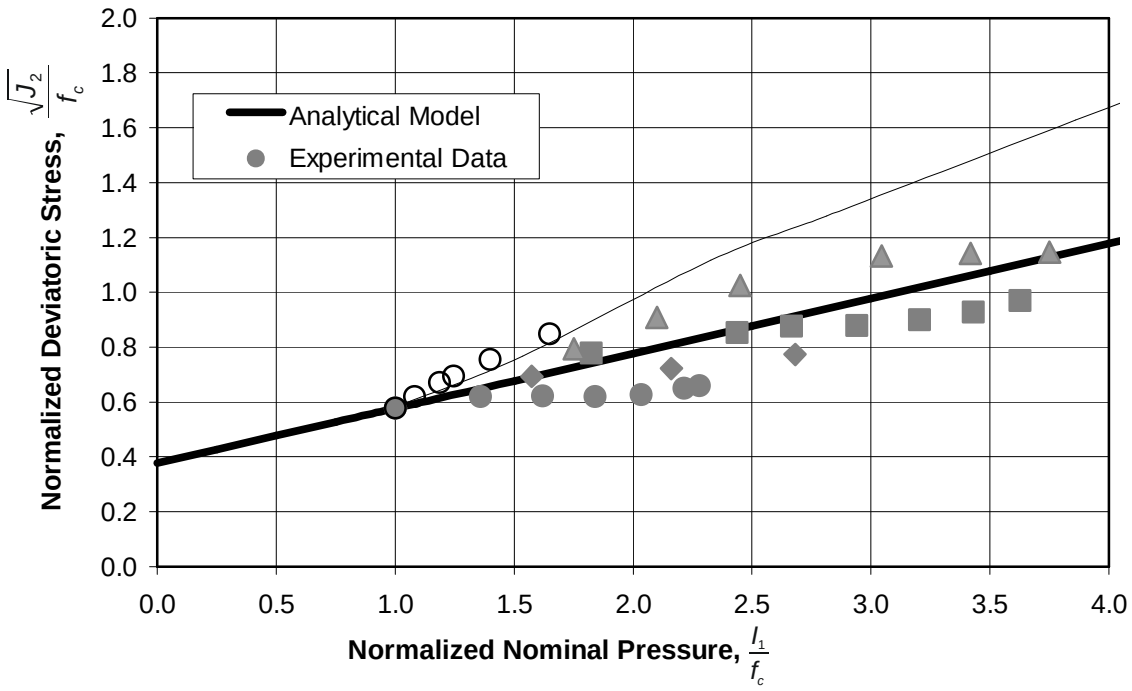

Figure 2.31:Maximum Normalized Deviatoric Stress Versus Nominal Pressure as Predicted and as Observed (Data as Presented in Figure 2.11)

The sensitivity of analyses to mesh discretization is a relevant issue for concrete loaded in compression and tension. Figure 2.33 shows the stress-deformation response for concrete subjected to uniaxial, monotonically increasing tensile loading as predicted using increasingly refined meshes in which the strength of the first element is reduced slightly to localize the damage mechanism. These data show that the introduction of the characteristic length and calibration of the element stress-strain relationship on the basis of the element characteristic length and concrete tensile fracture energy essentially eliminates dependence on mesh size.

Figures 2.34 and 2.35 show the stress-deformation response for concrete subjected to uniaxial, monotonically increasing compressive loading. Figure 2.34 shows results for analysis of a concrete prism with increasingly refined meshes in which the strength of the first element is reduced slightly to localize the damage mechanism. As with the tensile analysis, introduction of a characteristic length and consideration of energy dissipation

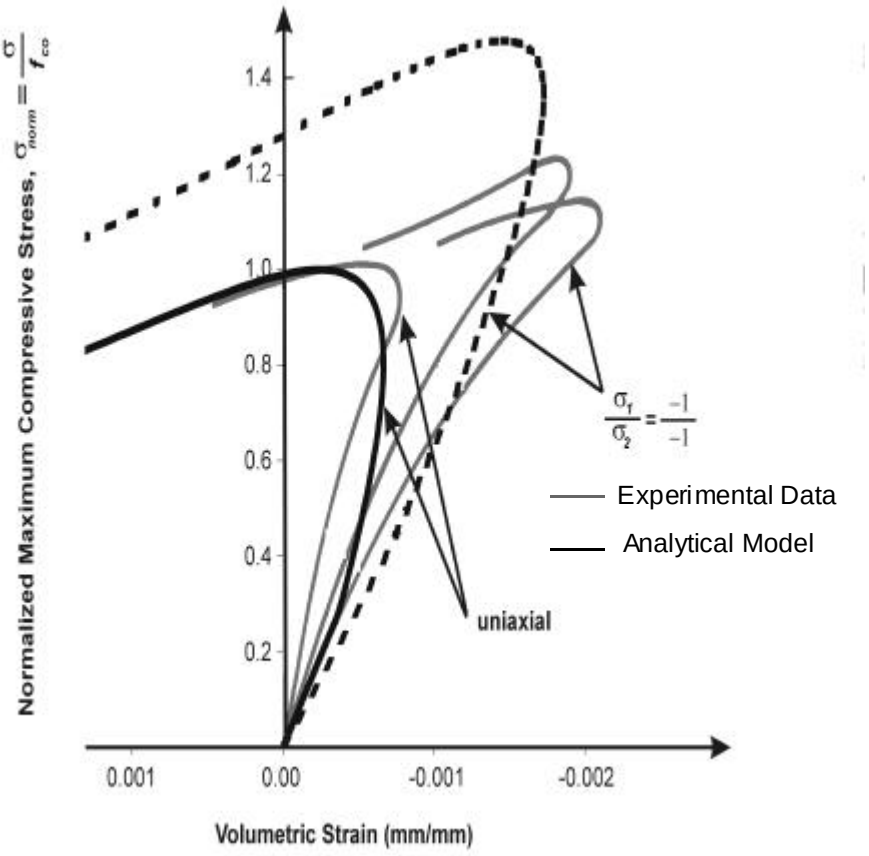

Figure 2.32:Predicted and Observed Compressive Strength Versus Volumetric Strain (Data as Presented in Figure 2.14)

under compressive softening produces analytical results that are essentially independent of mesh discretization. Figure 2.35 shows the stress-strain response for variable length concrete specimens modeled using a single element, these results show that the strain history in the softening regime is a function of the element length. These results support experimental observation that concrete elements of decreasing length show increasing strain ductility [van Mier, 1986].

2.6 Conclusions

The concrete constitutive model proposed for use in this investigation characterizes the observed response of plain concrete in reinforced concrete beam-column bridge joints subjected to earthquake loading. Plain concrete is modeled as a continuum, and plasticity theory and damage theory are employed to develop an analytical model that characterizes

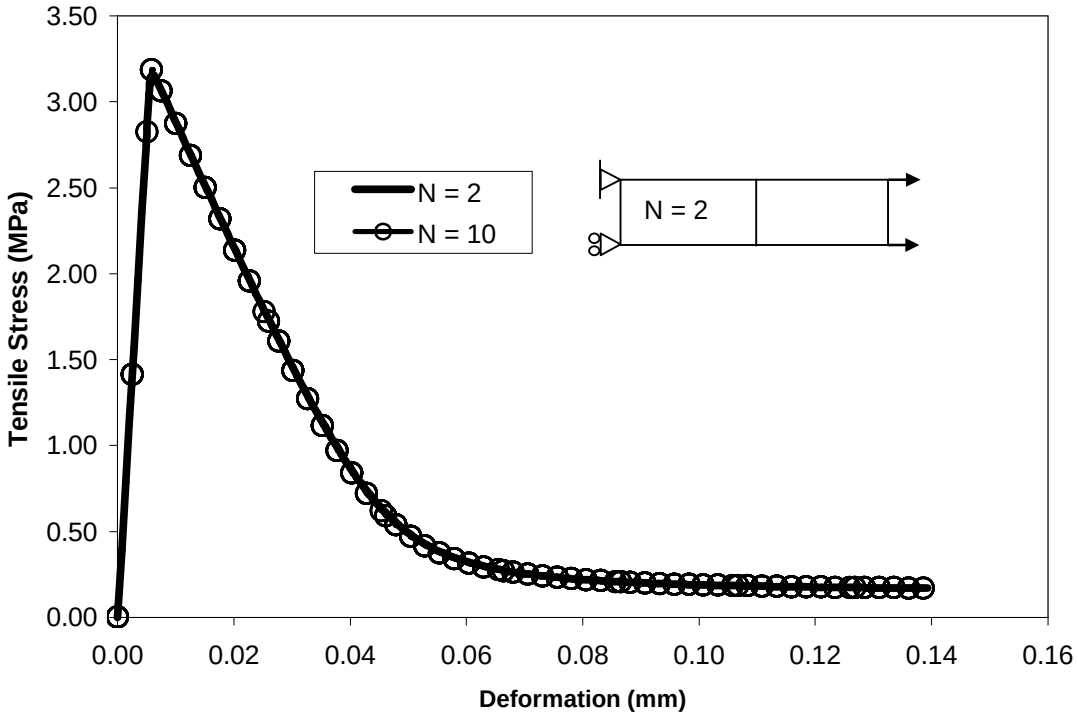

Figure 2.33:Predicted Tensile Stress-Strain Response for Variable Mesh Size

the response of plain concrete subjected to variable load histories. The result of experimental testing of reinforced concrete structural elements are used as a basis for further refinement of the model. Variability in concrete material response within individual experimental investigations and between studies requires that an appropriate analytical model predict the fundamental characteristic of the material response rather than the results of a particular investigation. Comparison of predicted and observed concrete response shows that the model proposed for this investigation characterizes the response of plain concrete within the appropriate range of loading for concrete composing reinforced concrete bridge frames. The model incorporates the characteristic length technique to ensure that the results are independent of mesh size.

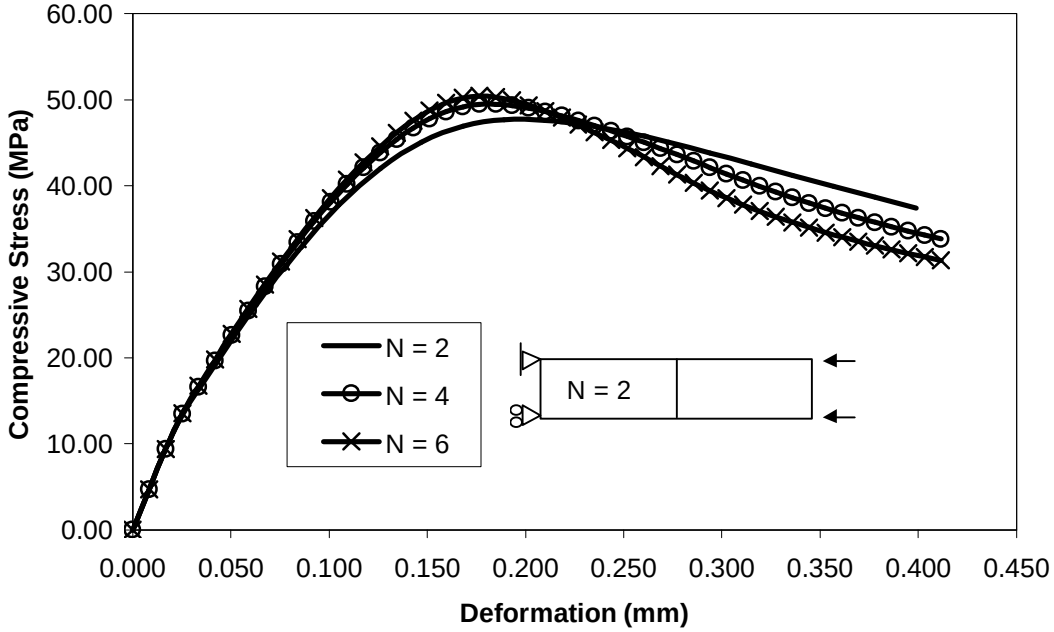

Figure 2.34:Insensitivity of Model to Mesh Discretization as Shown by Predicted Concrete Compression Stress-Strain History for Variable Mesh Sizes

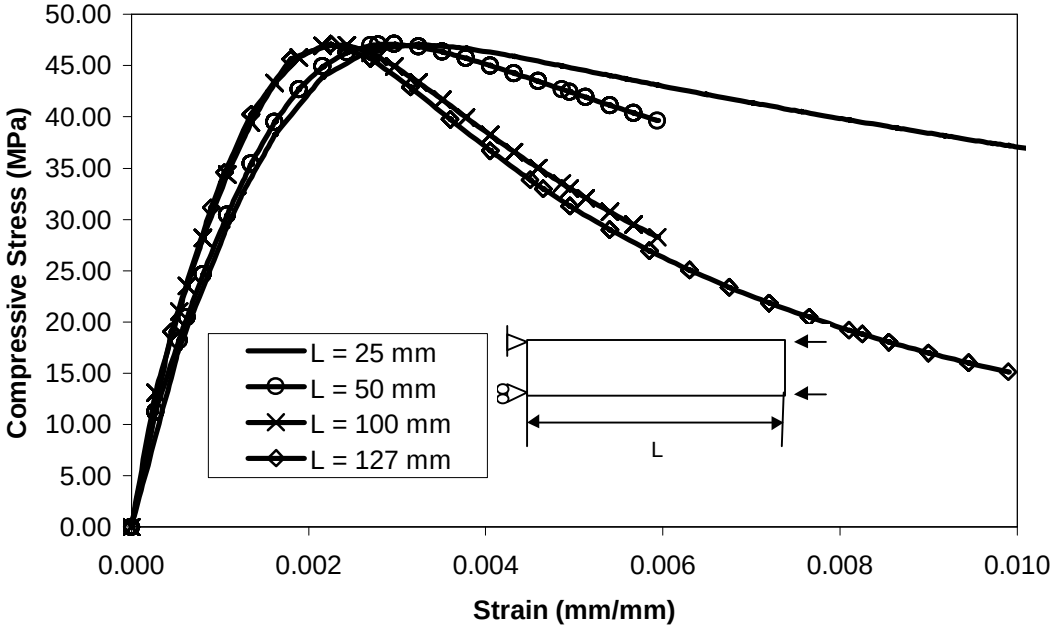

Figure 2.35:Averaging of Concrete Damage under Compressive Loading as Shown by the Predicted Compression Stress-Strain History for Variable Length Elements